frontiers | Frontiers in Materials

TYPE Review
PUBLISHED 13 August 2025
DOI 10.3389/fmats.2025.1639589

OPEN ACCESS

EDITED BY
Xingtao Xu,
Zhejiang Ocean University, China

REVIEWED BY
Raphael Mmaduka Obodo,
University of Nigeria, Nigeria
Yunhu Hu,
Huainan Normal University, China

*CORRESPONDENCE
Yin Yu,
dy_rainy@163.com

†These authors have contributed equally to this work

RECEIVED 04 June 2025
ACCEPTED 18 July 2025
PUBLISHED 13 August 2025

CITATION
Tang L, Wei T, Wei Y, Yu Y and Zhang H (2025) Research advances in carbon-based electrode materials for electrosorptive separation of uranium from aqueous solutions. *Front. Mater.* 12:1639589. doi: 10.3389/fmats.2025.1639589

Research advances in carbon-based electrode materials for electrosorptive separation of uranium from aqueous solutions

Ling Tang[1†], Tao Wei[1], Yanfeng Wei[1†], Yin Yu[2*†] and Haipeng Zhang[1]

[1]State Key Laboratory of Heavy Oil Processing at Karamay, Department of Engineering, China University of Petroleum-Beijing at Karamay, Karamay, China, [2]Xinjiang Academy of Environment Protection Science, Urumqi, Xinjiang, China

Electrosorptive removal of uranium from aqueous solutions has emerged as an auspicious approach for mitigating radioactive pollution, with carbon-based materials serving as pivotal electrode components due to their exceptional conductivity, tunable surface chemistry, and structural versatility. This review thoroughly examines recent progress in carbon-based capacitive deionization (CDI) electrodes for U(VI) removal and systematically assesses critical modification approaches, including heteroatom doping, surface functional group modification, and metal oxide loading. Each strategy is critically examined regarding its underlying mechanism, material design principles, and influence on uranium adsorption capacity and selectivity. A particular emphasis is placed on synergistic effects from combined modification approaches, which consistently outperform single-component systems. Bridging insights from environmental science and energy storage technologies, this work proposes an integrated optimization framework that establishes fundamental structure-performance relationships for CDI electrodes. By systematically synthesizing current research progress while identifying key knowledge gaps, this review offers strategic guidance for the rational design of next-generation carbon-based materials to enable efficient, selective, and sustainable radioactive wastewater remediation.

KEYWORDS

uranium, electrosorption, carbon-based electrodes, water treatment, electrode modification

1 Introduction

Uranium, a naturally occurring radioactive heavy metal, is ubiquitously distributed in geological matrices such as rocks and soils (Othman and Hussein, 2025). Still, its release into the environment becomes more pronounced during the nuclear fuel cycle and related industrial activities (Dong et al., 2025). This is particularly evident during key stages such as uranium mining and refining (Schneider et al., 2013), ore leaching (Wang N. et al., 2024), tailings management (Chen et al., 2022), fuel fabrication (Hansson et al., 2017), and post-irradiation processing (Van Zile et al., 2024). Typical sources of uranium contamination include process wastewater generated from acid or alkaline leaching in uranium mining

operations (Ning et al., 2021), leachates originating from tailings impoundments (Xie et al., 2025), high-level liquid radioactive waste produced during spent fuel reprocessing (Wang et al., 2024b), and the improper storage or disposal of other uranium-bearing radioactive materials (Gomes et al., 2012). These sources collectively contribute to elevated uranium concentrations in surrounding groundwater and surface water, often exceeding regulatory safety limits (Xie et al., 2025). Uranium-contaminated water posed not only radiological hazards, but also chemical risks due to the high mobility and nephrotoxicity of the hexavalent uranyl ion (UO_2^{2+}) (Bala et al., 2022). It can readily disperse through aquatic systems and bioaccumulate along the food chain, thereby posing long-term threats to both ecosystems and human health (Gavrilescu et al., 2009). In response to the ecological threats posed by uranium contamination in aquatic environments, many countries have established stringent regulatory standards for radioactive pollutant discharge. For instance, China's Law on the Prevention and Control of Radioactive Pollution explicitly restricts the discharge of uranium-containing wastewater and encourages the development of efficient uranium removal technologies to safeguard water quality and environmental safety.

Currently, the commonly employed techniques for uranium removal from aqueous solutions include conventional methods such as chemical precipitation (Song et al., 2024), ion exchange (Dong and Brooks, 2006), adsorption (Zhu S. et al., 2018), and membrane separation (Misra et al., 2009). Although these methods have been applied in practical engineering scenarios to some extent, they still suffer from several inherent limitations. For example, chemical precipitation requires large amounts of reagents and generates radioactive sludge; ion exchange and adsorption often exhibit low selectivity and poor regenerability of the sorbents, while membrane separation is prone to fouling and typically involves high operational costs (Ke et al., 2023). In recent years, emerging electrochemical separation technologies have garnered considerable attention (Wang et al., 2024a). Among them, capacitive deionization (CDI), as a representative electrosorption technique,has been recognized as a promising candidate for uranium removal from aqueous media due to its distinct advantages, including low energy consumption, high efficiency, operational simplicity, excellent regenerability, and environmental friendliness (Tang et al., 2025; Tauk et al., 2024; Wang S. et al., 2025). CDI operates by applying a low voltage across a pair of porous electrodes, driving cations toward the cathode and anions toward the anode (Figure 1A). These ions are subsequently accumulated within the electric double layers (EDLs) formed along the surfaces of the electrode pore structures (Figure 1B), thereby enabling the electro-sorption and removal of target ions from the solution (Wu et al., 2024). This process does not require the involvement of additional chemical reagents, thereby avoiding the introduction of secondary contaminants (Tauk et al., 2024). Moreover, the electrode materials can be readily regenerated and reused through voltage-assisted desorption (Shehzad et al., 2024). Benefiting from the aforementioned mechanisms, CDI has demonstrated great potential in water treatment. Studies have shown that, compared with conventional techniques such as chemical precipitation, CDI offers several advantages for the remediation of uranium-contaminated water, including reagent-free operation, reduced waste generation, and efficient removal and recovery of uranium ions (Cao et al., 2023; Liu et al., 2024b). Therefore, CDI is regarded as one of the most promising and innovative technologies for the future remediation of uranium-contaminated water.

In capacitive deionization systems for uranium removal, the performance of electrode materials is crucial (Zhao et al., 2025). Among various electrode materials, carbon-based materials have emerged as one of the most promising candidates for capacitive deionization-based separation of U(VI), owing to their outstanding electrical conductivity, high specific surface area, excellent chemical stability, and tunable surface functional groups (Cheng et al., 2024; Liu et al., 2022). Recent advances in carbon-based materials have demonstrated significant potential for uranium electrosorption applications. Liu et al. developed graphene oxide electrodes via electrochemical deposition on carbon felt, achieving a U(VI) adsorption capacity of 301.0 mg/g at 1.2 V with excellent regeneration stability (Liu D. et al., 2024). Their subsequent work fabricated GO/polypyrrole hybrid films through one-step electrodeposition, exhibiting enhanced conductivity and rapid adsorption equilibrium within 60 min (Liu et al., 2024c). Ren et al.synthesized malonamide–amidoxime-functionalized GO nanocomposites, showing exceptional U(VI) uptake (479.4 mg/g at pH 4.5) with fast kinetics (Ren et al., 2024). Further improvements were achieved through nitrogen-doped GO aerogels, reaching a record capacity of 680.89 mg/g, and 3D GO/PEI monoliths (Ren et al., 2025a; Ren et al., 2025b) with enhanced hydrophilicity and amine-rich coordination sites.

Parallel developments in supercapacitor materials offer valuable insights for electrosorption. Obodo et al. demonstrated that GO-supported binary and ternary metal oxides (e.g., MnO_2@NiO/graphene, CuO@NiO@ZnO/GO) exhibit high specific capacitance (up to 1350 F g^{-1}) and cycling stability, attributed to optimized redox activity and conductive frameworks (Obodo et al., 2022a; Obodo et al., 2022b; Obodo et al., 2024a). MXene-GO hybrids further enhance conductivity and ion diffusion (Naz et al., 2025). These advances highlight the potential for designing high-performance uranium electrosorption electrodes through tailored structural engineering and interfacial optimization.

Despite the growing attention on carbon-based materials for uranium electrosorption, current research still lacks a unified framework that systematically integrates structural engineering, surface chemistry, and electrochemical functionality. Most prior studies have focused on individual modification strategies—such as heteroatom doping, surface functionalization, or metal oxide loading—without adequately investigating their synergistic effects or translating insights from related fields like supercapacitors into environmental remediation. To address these gaps, this review presents a comprehensive overview of three primary optimization strategies for carbon-based electrodes: heteroatom doping (Section 4), functional group modification (Section 5), and metal oxide loading (Section 6). The discussion centres on the underlying mechanisms by which each approach enhances U(VI) adsorption capacity, selectivity, and electrochemical stability. Particular emphasis is placed on the synergistic application of these strategies, which has emerged as a key innovation for improving the overall efficiency of capacitive deionization systems. By integrating advances in material design with insights from energy storage research, this review provides a holistic perspective on developing high-performance electrode materials for uranium removal from aqueous environments.

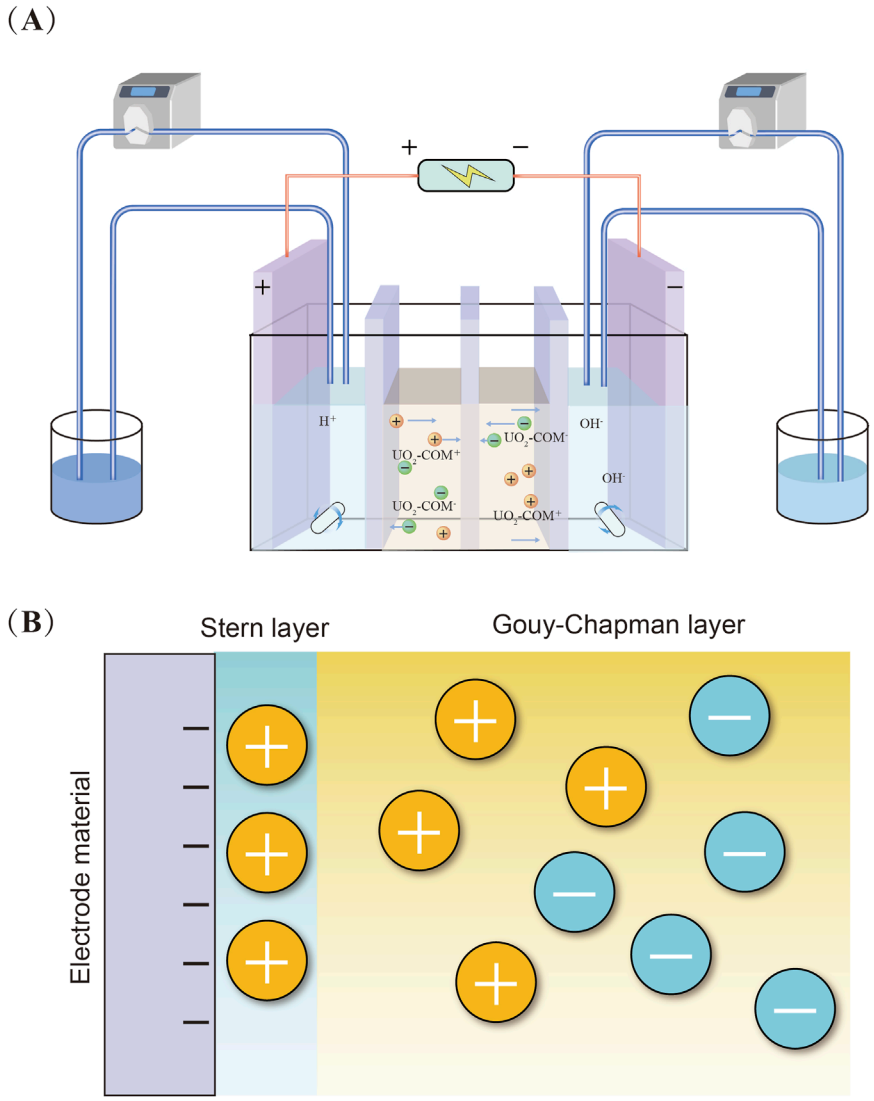

FIGURE 1
Schematic illustration of **(A)** the CDI device and **(B)** the Gouy-Chapman-Stern model.

2 Classifications of carbon-based materials for electrosorption applications

Owing to their excellent electrical conductivity, porous structure, chemical stability, and surface tunability (Zhang C. et al., 2018; Zhang et al., 2019), carbon-based materials have been widely employed in uranium-specific applications such as the treatment of uranium-containing wastewater, environmental remediation of uranium pollution, uranium extraction from seawater, and uranium resource recovery. As illustrated in Figure 2A, the number of related research studies has shown a steady year-on-year increase, underscoring carbon-based materials as the most promising class of electrode candidates for capacitive deionization-based separation of U(VI). Particularly under aqueous conditions, the migration behavior of uranyl ions (UO_2^{2+}) is constrained by their hydration shell structure, charge density distribution, and pore-size compatibility (Kerisit and Liu, 2013). Therefore, adsorbent materials are required to provide not only efficient mass transport pathways and a stable interfacial coordination environment, but also a certain degree of selective recognition capability (Zhu et al., 2025). Compared with other types of electrode materials, carbon-based materials exhibit a highly tunable synergy among structure, electrical conductivity, and functional sites. This enables them to achieve superior overall performance in the electrosorption of U(VI), typically characterized by fast kinetics, high adsorption capacity, and excellent structural stability (Mahmoud et al., 2023; Mittal et al., 2024).

According to differences in carbon framework morphology, dimensional architecture, pore distribution, and surface reactivity, carbon-based materials commonly employed in U(VI) electrosorption studies can be broadly classified into five major categories: activated carbon (Giraldo et al., 2025), graphene and its oxides (Duster et al., 2017), carbon nanotubes (Li et al.,

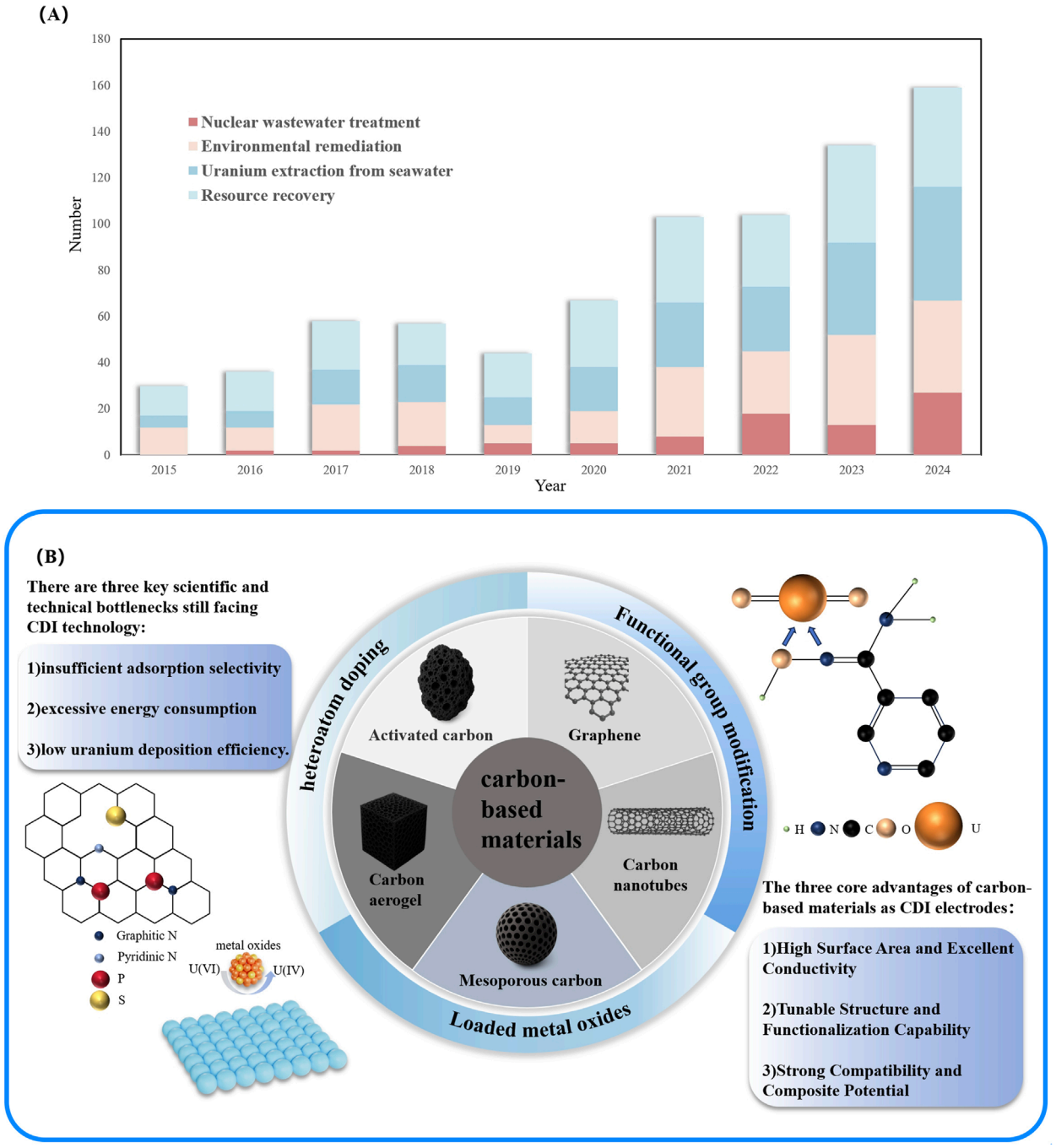

FIGURE 2
(A) Number of publications from 2015 to 2024 with the keywords "carbon-based material". Source: Scopus, access on 19 April 2025. **(B)** Types and optimization strategies of carbon-based materials commonly used for uranium removal by CDI techniques.

2024), mesoporous carbon (Zhang C. et al., 2018), and carbon aerogels (Zhang et al., 2019) (Figure 2B). Because graphene and its oxides have shown higher overall research activity than carbon nanotubes in recent years, particularly in areas such as interfacial coordination mechanisms, surface functionalization strategies, and the construction of composite electrodes, this section has been moderately adjusted to introduce graphene-based systems first, to better reflect the current mainstream trend in research. These five types of materials represent distinct spatial configurations, ranging from zero-dimensional particles to one-dimensional tubular structures, two-dimensional layered frameworks, and three-dimensional network architectures. Each exhibits specific advantages and limitations in terms of mass transfer pathways, charge distribution, and interfacial reaction mechanisms. This section provides a systematic overview of the adsorption performance of these carbon-based materials, summarizing

their structural characteristics, adsorption mechanisms, and experimental behaviors in sequence. Particular emphasis is placed on elucidating the coupling relationship between material structure and uranium affinity, which serves as a theoretical foundation for subsequent optimization strategies.

2.1 Activated carbon

Activated carbon (AC) is a representative class of porous carbon materials, typically prepared from biomass or coal through high-temperature carbonization followed by activation. It features a highly developed pore structure and a large specific surface area (Giraldo et al., 2025). The combination of micropores (<2 nm) and mesopores (2–50 nm) forms a well-developed pore network, and the specific surface area typically ranges from 500 to 2000 m^2/g (Giraldo et al., 2025; Zhang C. et al., 2018). A high specific surface area enables activated carbon to provide sufficient electric double-layer storage space, which is beneficial for enhancing electrosorption capacity. Meanwhile, the presence of hierarchical pores helps alleviate ion diffusion resistance and improves adsorption kinetics (Zhou et al., 2022). In practical measurements, the BET specific surface area of activated carbon prepared from different raw materials typically ranges from several hundred to over one thousand square meters per Gram. For example, the specific surface area of corn cob-derived activated carbon (Giraldo et al., 2025) can be increased from 563 to 1395 m^2/g after activation.

Recent studies have reported the use of various agricultural and forestry wastes, such as palm shells (Youssef et al., 2024), betel nut residues (Liu et al., 2016), and hazelnut shells (Zhu et al., 2021), as precursors for activated carbon production. After treatment with activating agents such as phosphoric acid, $ZnCl_2$, or NaOH under appropriate process conditions, these materials can be converted into structurally stable and surface-active adsorbents. The framework of activated carbon is primarily composed of sp^2–hybridized carbon, which imparts a certain degree of electrical conductivity and facilitates the formation of conductive pathways within the electrode. Overall, activated carbon features a mature and stable structure, broad availability, and low cost, and has already been widely applied in CDI for desalination. The removal of uranyl ions (UO_2^{2+}) by activated carbon primarily relies on its well-developed pore structure and the inherent oxygen-containing functional groups on its surface. Micropores serve as physical enrichment sites for uranyl ions, enabling U(VI) to preferentially enter and be captured within the pore channels under an applied electric field. Meanwhile, mesopores act as transport pathways that facilitate the migration of uranyl ions from the bulk solution to the adsorption sites, thereby enhancing adsorption kinetics (Guo et al., 2025; Wang Z. et al., 2025). In addition, the surface of activated carbon typically contains a certain amount of functional groups such as carboxyl, hydroxyl, and carbonyl groups, which originate from incomplete carbonization of the precursor or are introduced during the activation process. These groups carry negative charges under neutral to mildly acidic conditions, enabling them to initially bind with UO_2^{2+} via electrostatic attraction, followed by the formation of inner-sphere complexes through coordination interactions (Mishra et al., 2017; Morsy et al., 2019). This dual mechanism of "physical enrichment combined with chemical coordination" endows activated carbon with favorable kinetic responsiveness and ion recognition potential in electrosorption systems. Benefiting from these mechanisms, activated carbon materials exhibit satisfactory uranium adsorption performance and environmental adaptability. Activated carbon derived from various biomass sources typically achieves maximum U(VI) adsorption capacities in the range of 20–30 mg/g (Table 1).

Despite the advantages of activated carbon, such as structural maturity and wide availability, it still faces certain limitations in practical applications. For example, the distribution of intrinsic surface functional groups is often non-uniform, which results in relatively low recognition and selectivity toward UO_2^{2+} in complex multi-ion aqueous systems (Wang D. et al., 2025). Moreover, the saturated adsorption capacity is constrained by the density of surface-active sites, which may limit its effectiveness in treating uranium-contaminated wastewater with high concentrations (Elhefnawy and Elabd, 2024). To address the aforementioned limitations, it is often necessary to incorporate other materials or functionalize activated carbon to meet higher performance requirements. Nevertheless, as a benchmark material, activated carbon remains an indispensable component in CDI-based uranium removal due to its high porosity and structural stability. Its advantages in terms of cost-effectiveness and technological maturity are unmatched by most alternative materials (Li et al., 2023).

2.2 Graphene

Graphene is a two-dimensional, single-atomic-layer material composed of sp^2–hybridized carbon atoms, featuring a theoretical specific surface area of up to 2630 m^2/g along with excellent electrical conductivity and mechanical strength. In contrast, graphene oxide (GO) is a derivative of graphene functionalized with oxygen-containing groups such as carboxyl, hydroxyl, and epoxy groups, which are introduced onto its basal plane and edges (Duster et al., 2017). Due to the presence of oxygen-containing functional groups, graphene oxide (GO) exhibits superior hydrophilicity and stronger coordination ability toward metal ions. However, these functional groups significantly disrupt the sp^2-conjugated carbon network, leading to a considerable decrease in electrical conductivity compared to pristine graphene (Hilmi et al., 2024).While pristine graphene typically exhibits an electrical conductivity of around 10^4 S m^{-1}, even the most effectively reduced GO through a water–hydrothermal–microwave process only reaches 43.78 S m^{-1} (Suranshe and Patil, 2023). When employed as CDI electrode materials, graphene-based structures not only offer high electric double-layer capacitance that enhances ion adsorption capacity but also accelerate interfacial charge transfer and reduce interfacial resistance due to their excellent electrical conductivity, thereby improving the electrosorption kinetics (Cai et al., 2017; Kalfa et al., 2020; Liu K. et al., 2025). However, it should be noted that graphene sheets tend to aggregate and restack in aqueous media, and excessive stacking can significantly reduce the effective specific surface area and hinder the connectivity of ion transport pathways (Yousef et al., 2025), which represents one of the major structural challenges in the application of graphene-based materials.

TABLE 1 Summary of Uranium (VI) electrosorption performance of representative carbon-based materials under Varying experimental conditions.

Type	Name	Conditions				Capacity (mg/g)	Kinetics	Isotherms	References
		C_0 mg/L	ph	Time (min)	Temperature (K)	Adsorption capacity			
Activated carbon	CC	100	6	55	298	22.12	Pseudo-second order	Sips	Giraldo et al. (2025)
	Eucalyptus Wood Biochar	100	5.5	20	298	27.2	Pseudo-second order	Langmuir	Mishra et al. (2017)
	PBC	50	4.5	60	298	9.89	Pseudo-second order	Sips	Youssef et al. (2024)
	AACC	20	7	420	303.15	2.32	Pseudo-second order	Langmuir	Wu et al. (2020)
Graphene	GO-ACF	50	5.5	30	298	298	Pseudo-second order	Langmuir	Chen et al. (2013)
	GO-CS-P	118	5	15	293	779.44		Langmuir	Cai et al. (2017)
	GONRs-IV	60	4.5	1440	298	437.1		Langmuir	Wang et al. (2021)
	GONRs/CTS	50	5.5	30	298	320	Pseudo-second-order	Langmuir	Hu et al. (2020)
Carbon nanotubes	CNTs-PDA-PGMA-EDA	50	5	180	298	192.9	pseudo-second-order	Langmuir	Song et al. (2016)
	PN@CNT	300	5	240	298	851.6	Pseudo-second-order	Langmuir	Li et al. (2024)
Mesoporous carbon	MCMs		4	50	298	293.95	Pseudo-second-order	Langmuir	Zhang et al. (2018a)
	HAC			120	298	3.3	Pseudo-second-order	Langmuir	Morshedy et al. (2021)
	0.2AO-OMC	50	5	90	298.15	322.6	Pseudo-second-order	Langmuir	Zhang et al. (2018b)
Carbon aerogels	CA-PO_4	110	5.5	60	298	150.3	Pseudo-second-order	Langmuir	Zhang et al. (2019)
	GO-CNT Aerogel	200	5	540	298.15	80	Pseudo-second-order	Langmuir	Gu et al. (2015)
	C-	100	7	360	298	465.75	Pseudo-second-order	Langmuir	Zhu et al. (2024)
	CS-CCN2		5		298	307.5	Pseudo-second-order	Langmuir	Tang et al. (2025)
	nZVI@KGMC	200	5	60	298	720.8	Pseudo-second-order	Langmuir	Wang et al. (2022)

Compared with conventional activated carbon, graphene or graphene oxide (GO)-based materials exhibit significant potential in both adsorption capacity and kinetics. Chen et al. (Chen et al., 2013) fabricated a graphene oxide-activated carbon felt (GO-ACF) composite by electrophoretic deposition followed by thermal treatment to immobilize the GO nanosheets, achieving a maximum U(VI) adsorption capacity of 298 mg/g at pH = 5.5, which is markedly higher than that of pristine ACF (173 mg/g).

The study further indicated that under an applied electric field, the two-dimensional lamellar structure of the GO-ACF composite effectively facilitates the formation of ion transport pathways during the electrosorption process, thereby enhancing the adsorption capacity for uranyl ions. In addition, Cai et al. (Cai et al., 2017) developed a phosphorylated graphene oxide-chitosan composite (GO-CS-P), which exhibited a maximum U(VI) adsorption capacity of 779.44 mg/g at pH = 5.0 and 293 K, with an equilibrium time of only 15 min. Under the assistance of an external electric field, the negatively charged phosphate groups further enhanced the electrosorption selectivity toward uranyl ions. These findings demonstrate that graphene-based materials not only provide abundant adsorption sites through their two-dimensional structure but also effectively improve adsorption capacity and selectivity in electrosorption systems by tuning the electric field and surface functional groups, highlighting their promising potential in electro-assisted uranium removal applications.

Overall, GO and its derivatives exhibit several advantages in the electrosorption of U(VI): (1) their large specific surface area and high electron mobility facilitate rapid electrosorption kinetics; (2) their surface properties are highly tunable, allowing for the modulation of uranium affinity through functional group modification; and (3) they can be integrated into three-dimensional structures such as gels and membranes, thereby enhancing their adaptability for practical engineering applications (Dubey et al., 2014). However, several limitations remain: (1) GO exhibits limited structural stability under strongly acidic conditions or high applied voltages (Jing et al., 2024); (2) the interlayer charge-shielding effect may obstruct access to active adsorption sites (Fan et al., 2025); and (3) GO sheets tend to aggregate under an external electric field, leading to a reduction in effective specific surface area, thereby necessitating the use of auxiliary materials or structural fixation strategies to construct stable three-dimensional conductive networks (Chen et al., 2013; Hu et al., 2020).

2.3 Carbon nanotubes

Carbon nanotubes (CNTs) are hollow one-dimensional tubular structures formed by the curling of sp^2-hybridized carbon atoms, typically classified into single-walled (SWCNTs) and multi-walled (MWCNTs) types. Owing to their excellent electrical conductivity, high mechanical strength, and remarkable chemical stability, CNTs provide low-resistance pathways for ion transport and efficient channels for electron conduction (Ji et al., 2022; Zhang X. et al., 2022). These unique features endow CNTs with distinct advantages in the electrosorptive removal of heavy metal ions.The adsorption of U(VI) by carbon nanotubes (CNTs) primarily involves three synergistic mechanisms: (1) the delocalized π-electron cloud distributed along the CNT surface enables weak non-covalent interactions with UO_2^{2+}, such as π-cation interactions and van der Waals forces, leading to initial physical enrichment; (2) the hollow structure of multi-walled CNTs (MWCNTs) provides a nanoconfined environment that facilitates the short-term accumulation of UO_2^{2+} under dynamic solution conditions; and (3) the presence of oxygen-containing functional groups (e.g., carboxyl, hydroxyl), as well as intrinsic structural defects on the CNT framework, enables coordination with U(VI), thereby enhancing adsorption selectivity (Ji et al., 2022; Li et al., 2024; Song et al., 2016).

Li et al. (2024) constructed a PN@CNT composite via a covalent anchoring strategy using phosphorus nitride imide (PN), which significantly enhanced the selective recognition and electrosorption performance toward U(VI). Under an applied voltage of 1.2 V in a uranyl solution (initial concentration: 100 mg/L, pH = 5.0), the material achieved a remarkable U(VI) adsorption capacity of 1006.9 mg/g within 60 min, far surpassing that of unmodified CNTs (only 228.9 mg/g). Mechanistic analysis revealed that the P=O and N-H sites in the PN molecules acted as Lewis bases to form dual coordination interactions with UO_2^{2+}, which, coupled with the excellent electronic conductivity of CNTs, established a synergistic "electron acceleration-coordination capture" dual-channel adsorption pathway, thereby significantly improving both uranium affinity and kinetic responsiveness of the material.

In addition to its adsorption performance, CNT also exhibits excellent engineering adaptability. Its one-dimensional fibrous structure is well-suited for the fabrication of novel reaction interfaces such as electrosorptive membrane electrodes and electrospun nanofibers (Chen et al., 2024), and it can be integrated with magnetic components to enable facile recovery and reuse of the material (Ahmad et al., 2020). However, certain limitations remain inherent to CNTs, such as their tendency to aggregate in aqueous media and their strong hydrophobicity, which lead to poor dispersion, reduced utilization of specific surface area, and limited exposure of surface-active sites. Moreover, the pristine CNT surface lacks sufficient functional groups, resulting in relatively low adsorption selectivity (Li et al., 2024). Consequently, CNTs primarily serve as electron transport pathways and structural frameworks in U(VI) removal, and are frequently integrated with functional ligands or metal oxides to construct high-performance composite electrodes (Zhang J. et al., 2024), making them one of the key functional components in electrosorption systems.

2.4 Mesoporous carbon

Mesoporous carbon (MC) has attracted increasing attention in the electrosorptive removal of aqueous U(VI) due to its tunable mesopore structure, high specific surface area, and excellent structural stability. With typical pore diameters ranging from 2 to 50 nm, MC can be precisely synthesized via hard-template methods (Zhang X. et al., 2023) or soft-template strategies (Liu et al., 2023), exhibiting well-defined diffusion pathways and favorable interfacial affinity toward uranyl ions. Compared with materials such as activated carbon and carbon nanotubes, mesoporous carbon exhibits a stronger capability for coordinated control of diffusion and reaction processes. Its well-ordered mesoporous network significantly reduces the mass transfer resistance of U(VI) within the pore channels, thereby enhancing both the adsorption rate and capacity (Song et al., 2018; Zhang C. et al., 2018). In addition, the surface of MC is enriched with oxygen-containing functional groups such as carboxyl and hydroxyl groups, which can form stable inner-sphere complexes with uranyl ions and thus improve both selectivity and binding stability (Kim et al., 2010). This combination of structural diffusion facilitation and interfacial chemical affinity

constitutes the fundamental mechanism for the efficient removal of U(VI) by mesoporous carbon.

Zhang C. et al. (2018) synthesized mesoporous carbon materials (MCMs) with an ordered mesoporous structure via a hard-template method and investigated their electrosorptive performance for U(VI) removal. The results showed that the maximum U(VI) adsorption capacity reached 293.95 mg/g at pH = 4. XPS analysis indicated that oxygen-containing functional groups such as carboxyl and hydroxyl groups participated in the coordination process with U(VI), as evidenced by the appearance and shifts of characteristic peaks in the U 4f spectra. These functional groups not only served as adsorption sites for uranyl ions but may also act as electron donors during electrosorption, thereby facilitating interfacial charge transfer and enhancing the adsorption performance. In addition, the mesoporous architecture provided ion transport pathways for uranyl ions, which effectively reduced mass transfer resistance under an applied electric field and improved the adsorption rate. The study further pointed out that the synergistic effect of the ordered pore structure and the distribution of surface functional groups was fundamental to the excellent electrosorption performance of MCMs, offering new insights into the design of efficient materials for uranium removal.

Compared with other carbon-based materials, MC exhibits superior overall performance in terms of adsorption capacity, kinetic rate, and selectivity toward metal ions, making it highly suitable for constructing efficient electrosorption systems. However, the synthesis of MC is relatively complex, particularly for ordered mesoporous carbon, which requires the use of templates and involves high production costs and challenges in large-scale preparation. From a practical application perspective, simplifying the synthesis process, improving the yield, and reducing the cost are critical issues that need to be addressed (Kausar et al., 2024). In addition, the mechanical strength of MC is sometimes inferior to that of dense activated carbon, necessitating shaping techniques or the use of binders to ensure electrode stability (Zhang et al., 2021). Nevertheless, the structural advantages of MC have been well demonstrated in experimental studies, confirming its potential as a promising material for high-performance electrosorption applications.

2.5 Carbon aerogels

Carbon aerogels (CAs) are a class of carbon-based materials characterized by a three-dimensional network structure, ultrahigh porosity, and excellent electrical conductivity. In recent years, they have been extensively studied for the electrosorptive removal of U(VI) from aqueous solutions (Ren et al., 2025a). Their hierarchical pore architecture, including micropores, mesopores, and macropores, provides low-resistance pathways for efficient uranyl ion diffusion and interfacial reactions. The continuous carbon framework facilitates rapid electron transport within the electrode, reducing internal resistance and accelerating electron transfer and adsorption kinetics during the electrosorption process (Liu et al., 2024d). Moreover, the highly tunable surface chemistry of CAs enables the formation of stable coordination complexes with UO_2^{2+}, thereby enhancing both selectivity and adsorption capacity (Zhang et al., 2019).

Unlike powdered carbon materials, aerogels possess a continuously interconnected three-dimensional network of channels, featuring ultrahigh porosity (>95%) and low bulk density (<50 mg/cm^3). This structural advantage significantly reduces the diffusion resistance of UO_2^{2+} ions migrating from the bulk solution to the active sites (Zhang et al., 2019). Gu et al. (2015) fabricated a composite carbon aerogel with a three-dimensional network structure by combining graphene oxide (GO) and carbon nanotubes (CNTs), followed by freeze-drying and carbonization. The resulting material exhibited good structural stability and electrical conductivity, achieving a maximum U(VI) adsorption capacity of approximately 80 mg/g under conditions of pH = 5.0 and an initial uranium concentration of 200 mg/L. Despite the relatively limited types of surface functional groups, the aerogel demonstrated notable uranium removal performance, indicating that its structural features and pore distribution played a dominant role in the adsorption process.

It is worth emphasizing that the continuous conductive network formed by carbon aerogels can improve the uniformity of potential distribution across the electrode, thereby reducing polarization impedance and enhancing the material's responsiveness to the external electric field (Kohli et al., 2016; Ren et al., 2025a). This facilitates more efficient migration of UO_2^{2+} ions to the surface active sites. Based on the integrated structural and interfacial mechanisms described above, carbon aerogels exhibit a triple synergistic mechanism during the electrosorptive removal of U(VI), namely, structure-guided diffusion, functional group-mediated coordination, and framework-supported electron transfer. This mechanism not only explains the high adsorption efficiency observed under both static and flow-through conditions but also provides a theoretical basis for improving selectivity, reusability, and compatibility with electrode integration. Owing to these advantages, carbon aerogels are considered one of the most promising uranyl-affinitive platforms with high integration potential among current carbon-based adsorbent systems.

3 Enhancing electron transport efficiency

The electrical conductivity of carbon-based materials directly influences electron transfer and the reduction-immobilization efficiency of uranyl ions during the electrosorption process. Enhancing the electron transport rate aims to reduce the internal resistance of the electrode material, facilitate rapid charge exchange at the interface, and thereby accelerate adsorption kinetics while also promoting favorable conditions for potential Faradaic reduction reactions (Shuang et al., 2024; Zhang R. et al., 2023). One of the key strategies to achieve this goal is the incorporation of heteroatoms into the carbon framework via heteroatom doping. Through atomic-scale substitution or defect embedding, heteroatoms can systematically modulate the electronic structure, surface polarity, and local coordination environment of the carbon skeleton, thereby significantly enhancing the adsorption capacity, binding stability, and interfacial reaction kinetics toward UO_2^{2+} (Chen et al., 2018; Liu et al., 2020). Unlike simple surface coating, heteroatom doping typically forms stable covalently embedded structures, endowing carbon materials with robust and long-lasting intraframework

functional sites. Among various dopant elements, nitrogen (N) (Song et al., 2018), phosphorus (P) (Olchowski et al., 2023), and sulfur (S) (Liu et al., 2020) exhibit distinct modulation effects on the electronic structure and interfacial chemistry of carbon-based materials, owing to their significant differences in electronegativity, covalent radius, and valence electron configuration. Nitrogen doping introduces pyridinic and graphitic sites, which can provide lone pair electrons for stable coordination with U(VI) and significantly enhance the electronic conductivity of the material. Phosphorus atoms are commonly incorporated in the form of P=O and P-C bonds, which increase the surface polarity of carbon and promote the formation of coordination structures with uranyl ions, thereby improving binding affinity. Sulfur doping introduces C-S-C and S=O configurations, especially in defect regions or along the edges of the carbon framework, where localized electron-rich domains can form and facilitate U(VI) complexation and interfacial electron transfer (Figure 1B). Therefore, heteroatom doping not only expands the reactivity and selectivity of carbon-based materials but also provides mechanistic support and structural advantages for the design of high-performance electrosorption systems.

3.1 Nitrogen doping

The incorporation of nitrogen atoms into carbon-based materials has been widely recognized as an effective strategy to significantly enhance their adsorption capacity toward U(VI). This enhancement originates from the atomic-level modulation of the carbon framework's electronic structure, surface polarity, and local chemical environment induced by nitrogen doping. Specifically, due to its higher electronegativity (3.04) and smaller covalent radius, nitrogen incorporation disrupts the uniform charge distribution of the original sp^{2-}hybridized carbon lattice, leading to localized electron density redistribution and the formation of electron-rich regions (Song et al., 2018). Chen et al. (2018) verified this phenomenon through density functional theory (DFT) calculations. As shown in Figure 3(A_1-A_3), significant electron redistribution and charge accumulation occurred at the nitrogen sites after forming a bidentate coordination complex with UO_2^{2+}, confirming their excellent electron-donating capability. This electronic polarization not only enhances the electrostatic attraction between the carbon-based material and UO_2^{2+} but also destabilizes the hydration shell of uranyl ions, thereby lowering the diffusion energy barrier and improving the efficiency of initial interfacial contact. In addition, nitrogen doping introduces a variety of reactive sites on the carbon surface, including pyridinic, pyrrolic, graphitic, and amino-type nitrogen species. Pyridinic nitrogen, which participates in interactions through lone pair electrons, often serves as an inner-sphere coordination center for U(VI), and its binding mechanism follows a Lewis base-Lewis acid complexation pathway. Pyrrolic nitrogen, on the other hand, plays a significant role in enhancing the surface polarity of the material and improving the stability of uranyl adsorption (Jin et al., 2023).

In electrosorption or reduction-adsorption synergistic systems, nitrogen doping can also modulate the charge transfer behavior of carbon-based materials and enhance interfacial electron coupling. Zhang Q. et al. (2024) synthesized Co and N co-doped carbon nanosheet arrays (Co-N-C/CF) by *in situ* growth of precursor nanosheets on a carbon fiber substrate via a hydrothermal method, followed by high-temperature annealing under an ammonia atmosphere (Figure 4A). The resulting material exhibited a U(VI) reduction rate nine times higher than that of the undoped counterpart. This study demonstrated that graphitic nitrogen significantly accelerated the U(VI) reduction process in the photo-electrocatalytic system by improving the electrical conductivity of the carbon framework. Similarly, the Fe/N co-doped carbon spheres developed by Zhu K. et al. (2018) also achieved partial conversion of U(VI) to U(IV). XPS spectra confirmed the accumulation of U(IV) on the material surface, demonstrating the synergistic contribution of nitrogen doping to the reduction pathway. Notably, the material exhibited a high adsorption capacity of 232.54 mg/g within just 20 min (initial U(VI) concentration: 20 mg/L, pH 6.0, 283 K), which is significantly faster than the equilibrium times reported for most conventional carbon-based adsorbents (Table 2). This indicates that nitrogen doping not only contributes to the construction of static adsorption sites but also plays a role in modulating reaction energy levels and coupling electron transport pathways.

In addition, nitrogen doping often introduces electron-rich defect sites and polarized structures, which significantly enhance the selective coordination ability and charge responsiveness of carbon materials toward U(VI). This structural modulation not only facilitates the formation of high-affinity coordination sites but also improves the electrochemical stability and pseudocapacitive behavior of the material. The experimental results reported by Jin et al. (2023) support this mechanism. In the Mn-N co-doped carbon spheres they developed, pyridinic nitrogen served as the primary coordination site for U(VI), and the material achieved a high adsorption capacity of up to 194 mg/g under an applied voltage of 1.8 V, while maintaining good structural stability during prolonged operation. Moreover, the synergistic effect between nitrogen and manganese effectively facilitated the formation of electronic transport pathways, thereby enhancing charge transfer efficiency. In 1.0 M NaCl solution, both the CV curve at a scan rate of 90 mV/s (Figure 4B) and the GCD curves under various current densities (Figure 4C) demonstrated pronounced specific capacitance and pseudocapacitive characteristics, further confirming the excellent electrochemical responsiveness and energy storage capability of the material.

3.2 Phosphorus doping

As an effective atomic-scale modification strategy, phosphorus doping can systematically enhance the U(VI) adsorption performance of carbon-based materials by substituting lattice carbon atoms with heteroatoms, thereby regulating the electronic structure, interfacial polarity, and coordination capacity. Upon incorporation into the carbon framework, phosphorus atoms form C-P and P=O bonds. Due to their relatively low electronegativity (2.19) and large covalent radius, these phosphorus sites induce surface charge redistribution and create regions of electronic heterogeneity, which in turn strengthen the electrostatic attraction and surface reactivity toward the highly charged UO_2^{2+} species (Chen et al., 2018).

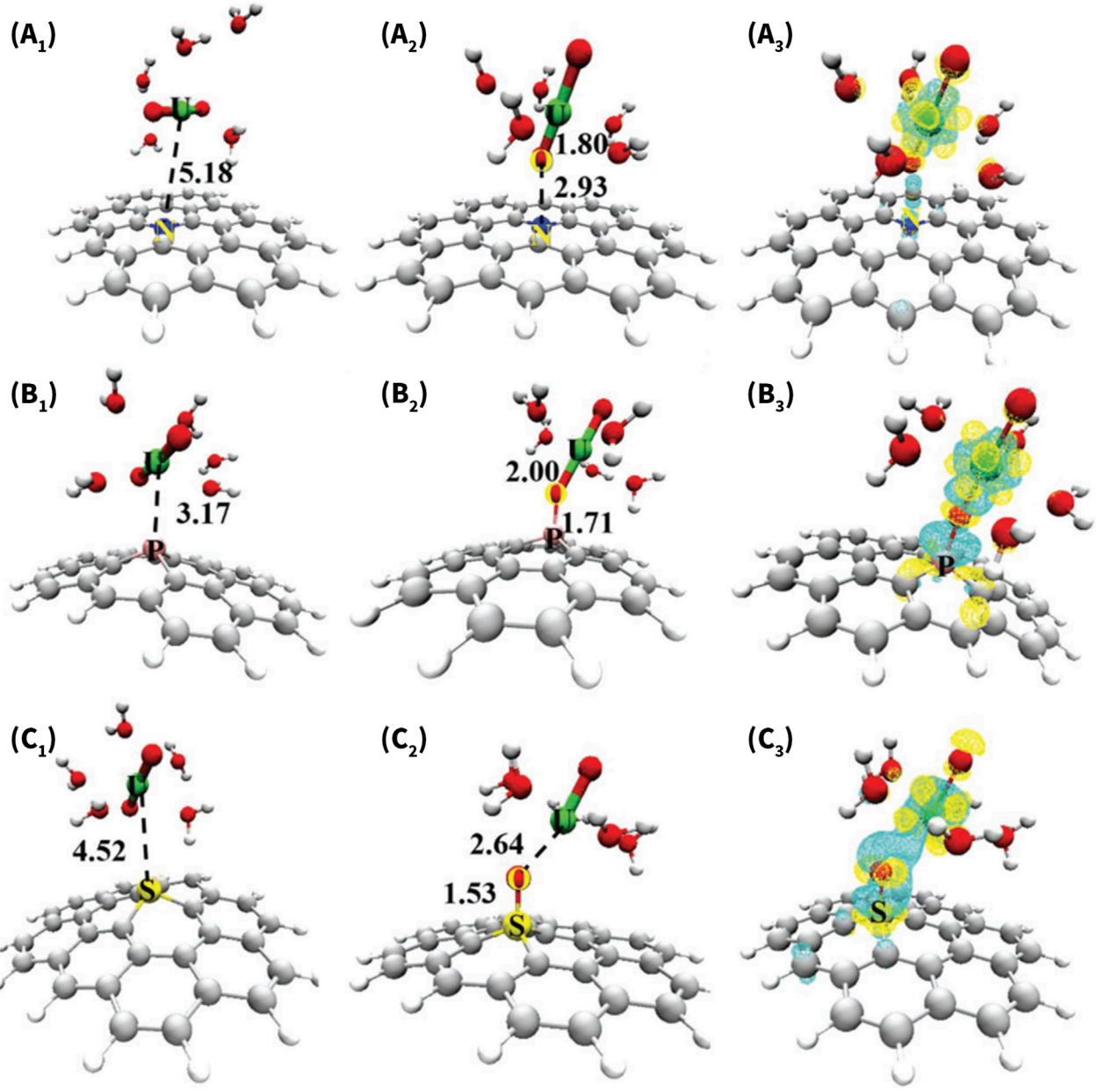

FIGURE 3
(A_1–C_1) Optimized structures of the G-X/Uranyl (U) complexes; **(A_2–C_2)** Optimized structures of the G-X/uranyl (O) complexes; **(A_3–C_3)** Charge density difference plot of the uranyl ion absorbed on the graphene surface substituted with the X atom, where X represents N, P, and S atoms, respectively. The yellow regions represent the electron accumulation and the light blue regions represent the electron deficiency. The isosurface has a value of 0.06 e $Bohr^{-3}$ (Chen et al., 2018).

In the study by Chen et al. (2018), XPS analysis revealed a significant attenuation of the P-O bonding signal after U(VI) adsorption, along with the emergence of a new U-O-P coordination peak, indicating the formation of a stable inner-sphere complex between U(VI) and phosphorus sites. Structural optimization and charge density difference analysis based on density functional theory (DFT) (Figure 4B_1-B_3) further confirmed that P-doped sites can form short coordination bonds with UO_2^{2+}, accompanied by pronounced charge redistribution, highlighting their strong complexation ability and electron coupling potential. In a competitive multi-metal system, the material exhibited remarkable selectivity toward U(VI) (Figure 4D). Moreover, the adsorption kinetics were significantly enhanced, with a removal efficiency of 80.5% achieved within 5 min (Figure 4E), and a maximum adsorption capacity of 294.16 mg/g at pH = 5, demonstrating that the incorporation of phosphorus sites not only improves binding stability but also effectively facilitates the adsorption process. In addition to providing strong coordination sites, phosphorus-doped carbon materials often exhibit improvements in structural porosity. For example, Liu et al. (2020) synthesized P-doped materials via

10.3389/fmats.2025.1639589

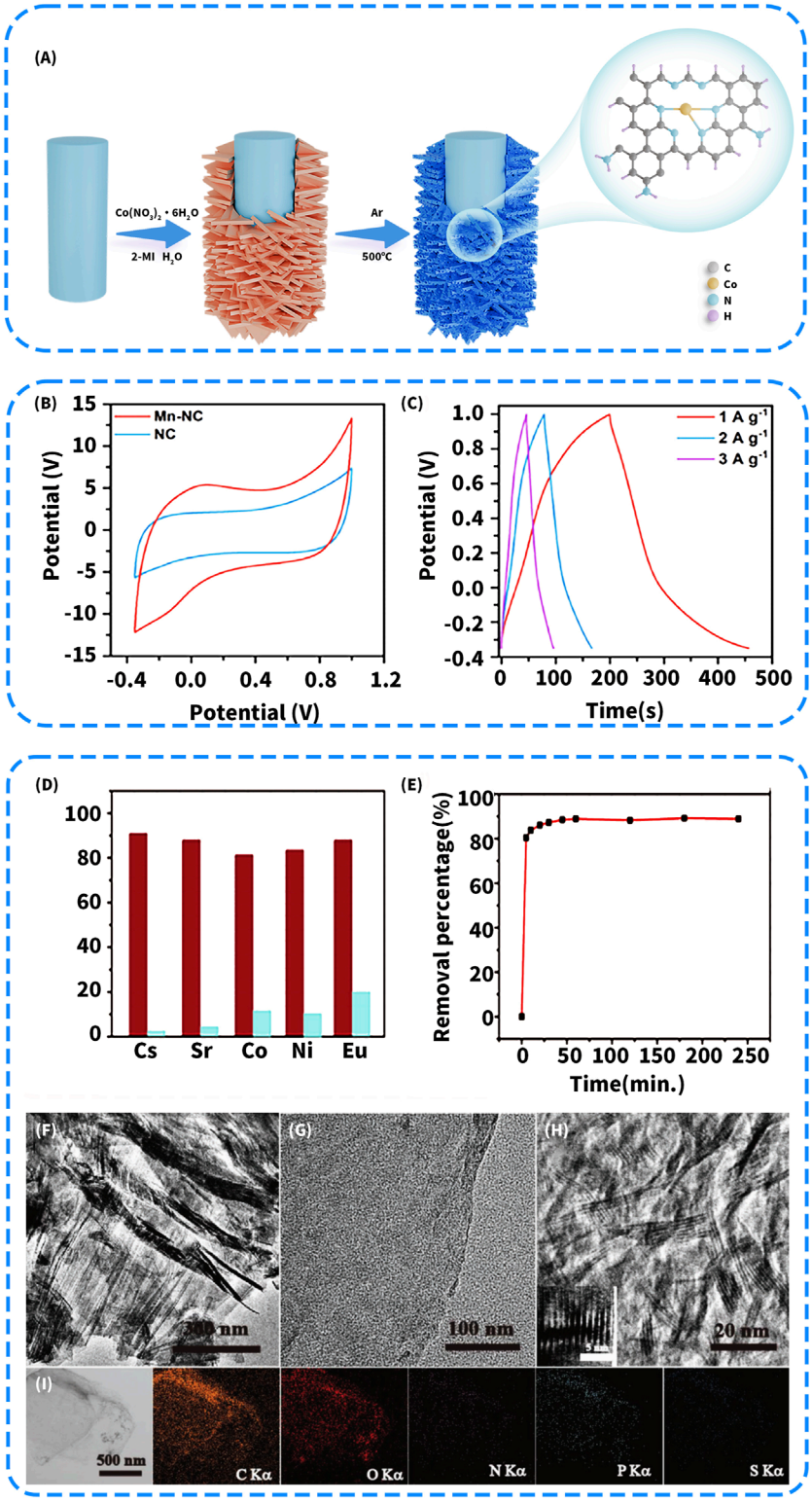

FIGURE 4
(A) Fabrication process of the Co-N-C/CF self-supporting cathode (Zhang Q. et al., 2024). **(B)** CV curves of samples in 1.0 M NaCl as the electrolyte at 90 mV/s; **(C)** GCD curves of Mn-NC at different current density (Jin et al., 2023). **(D)** Sorption percentages of U(VI) (red) and the competitive metal ions (blue) in the binary-metal systems; **(E)** Time-dependent removal of U(VI) on the NPS-GLCs (initial U(VI) concentration of 20 mg L^{-1}); **(F–H)** TEM and HRTEM images of NPS-GLCs; **(I)** Compositional EDS mapping of NPS-GLCs (Chen et al., 2018).

TABLE 2 Comparative performance of functionalized carbon-based electrode materials for Uranium (VI) removal via electrosorption: Effects of heteroatom doping, surface functionalization, and metal oxide loading.

Optimization strategies	Name	Conditions				Capacity (mg/g)	Kinetics	Isotherms	Reusability	References
		C_0 (mg/L)	ph	Time (min)	Temperature (K)					
Heteroatom doping	Mn-NC	500	—	—	—	194	Pseudo-second-order	—	After ten cycles, the adsorption capacity remained excellent	Jin et al. (2023)
	Co-N-C/CF-5	—	5.2	—	—	—	Pseudo-first-order	—	After twenty cycles, the removal rate is more than 93%	Zhang J. et al. (2024)
	Fe/N-C-700	20	6	20	283	232.54	Pseudo-second-order	Langmuir	After six cycles, the adsorption capacity is 197.66 mg/g	Zhu et al. (2018a)
	NPS-GLCs	20	5	30	298	294.16	Pseudo-second-order	Langmuir	—	Chen et al. (2018)
	amidate-CS	50	6	120	298	290.69	Pseudo-second-order	Langmuir	After five cycles, the adsorption capacity is more than 75%	Liu et al. (2020)
Surface functional group modification	0.2AO-OMC	50	5	90	298.15	322.6	Pseudo-second-order	Langmuir	After ten cycles, the adsorption capacity is 221.86 mg/g	Zhang et al. (2018b)
	AMG	1000	5	200	298	164.75	—	—	After five cycles, the adsorption capacity is 148.28 mg/g	Xue et al. 2021
	SWCNH-TETA	60	6	180	303	333.13	Pseudo-second-order	Langmuir	After five cycles, the removal rate is 87.2%	Wang et al. (2020)
	AOPEI-C-PAN fibers	50	7	2160	303	1738.5	Pseudo-second-order	Langmuir	After five cycles, the removal rate is more than 90%	Chen et al. (2024)
	WH-AO	10	4.5	1440	298	355.6	Pseudo-second-order	Langmuir	—	Jin et al. (2018)
	HCSs-300	50	7	25	298	179.95	—	Langmuir	After four cycles, the adsorption capacity is 46.14 mg/g	Zhang et al. (2013)

(Continued on the following page)

10.3389/fmats.2025.1639589

TABLE 2 (*Continued*) Comparative performance of functionalized carbon-based electrode materials for Uranium (VI) removal via electrosorption: Effects of heteroatom doping, surface functionalization, and metal oxide loading.

Optimization strategies	Name	Conditions				Capacity (mg/g)	Kinetics	Isotherms	Reusability	References
		C_0 (mg/L)	ph	Time (min)	Temperature (K)					
	LP@AC	10	5	720	303	1308.87	Pseudo-second-order	Langmuir	After six cycles, the removal rate is 85.77%	Jiao et al. (2023)
	P-Fe-CMK-3	20	4	30	298	150	Pseudo-second-order	Freundlich	After five cycles, the removal rate is more than 99%	Husnain et al. (2017)
Metal oxide loading	Fe_3O_4@COFs	10	7	30	298.15	492.6	Pseudo-second-order	Langmuir	After ten cycles, the removal rate is more than 80%	Yang et al. (2023)
	Fe_3O_4 @MBC	50	4.5	720	298	70.45	Pseudo-second-order	Langmuir	After three cycles, the removal rate is more than 83%	Chen et al. (2023)
	Fe_3O_4@C-KO	50	6	120	298	38.76	Pseudo-second-order	Langmuir	After three cycles, the removal rate is more than 80%	Liu et al. (2016)
	BC/α-MnO_2^{-2}	100	4	120	298	280.2	Pseudo-first-order	Langmuir	After five cycles, the removal rate is more than 90%	Liu et al. (2024a)
	TiO_2@MXene/CF	10	5	80	298	492.6	pseudo-second-order	Langmuir	After fifteen cycles, the removal rate is more than 97%	Guo et al. (2024)
	CF@TiO_2	10	5	30	298	—	—	—	After thirty cycles, the removal rate is more than 97%	Cai et al. (2024)

10.3389/fmats.2025.1639589

carbonization of a polyphosphazene precursor, which resulted in a typical layered microporous structure. The BET specific surface area increased from 70.31 m^2/g to 119.74 m^2/g. Furthermore, the material exhibited a high U(VI) adsorption capacity of 290.69 mg/g and demonstrated favorable diffusion kinetics and stability under mildly acidic conditions.

Compared with nitrogen doping, phosphorus doping has a relatively limited effect on improving the electrical conductivity of carbon materials, but it demonstrates superior selectivity and anti-interference capability in multi-ion systems. Studies have shown that phosphorus-modified activated carbon can still achieve a U(VI) adsorption capacity of 129.8 mg/g in the presence of coexisting ions such as Ca^{2+} and Mg^{2+} (Olchowski et al., 2023). This performance is attributed to the selective complexation of UO_2^{2+} by functional groups such as PO_3^{2-}, as well as the interfacial and thermal stability conferred by phosphorus-containing structures, which together enhance the cycling durability of the material.

3.3 Sulfur doping

Sulfur doping, achieved by incorporating sulfur atoms into the carbon lattice framework, has been demonstrated to significantly enhance the U(VI) adsorption capacity of carbon-based materials and has recently emerged as an important component of non-metallic heteroatom doping strategies. Sulfur has an electronegativity of 2.58, which is comparable to that of carbon (2.55), but its larger atomic radius and high polarizability allow it to modulate the local electronic environment and enhance interfacial reactivity. Sulfur atoms are typically embedded at the edges and defect sites of the carbon matrix in the form of thioether (C-S-C) or sulfonyl (C-SO_x) groups, contributing to electron-rich sites and promoting coordination with UO_2^{2+}. Due to the relatively large atomic radius of sulfur (approximately 102 p.m.), its incorporation into carbon frameworks often induces structural distortion, leading to the formation of additional pore sites and defects. The valence shell of sulfur atoms readily expands to form lone-pair electron clouds, resulting in electron-rich surfaces upon sulfur doping. This localized electron enrichment generates strong electrostatic attraction toward the positively charged UO_2^{2+} ions, thereby facilitating their accumulation near the material surface (Chen et al., 2018).

Chen et al. (2018) validated this concept through both structural characterization and theoretical simulation. Transmission electron microscopy (TEM) images revealed a layered stacking morphology composed of graphene-like nanosheets (Figures 4F–H), and high-resolution images displayed well-defined lattice fringes, indicating good crystallinity of the material. Elemental mapping analysis (Figure 4I) further confirmed the homogeneous co-doping of sulfur along with carbon, oxygen, nitrogen, and phosphorus, which provides a structural basis for subsequent electronic structure modulation and coordination-driven adsorption. In addition, density functional theory (DFT) calculations revealed the synergistic interaction mechanism between sulfur sites and U(VI). The S=O functional group can provide lone pair electrons to form stable coordination bonds, and as a "soft base" doping site, it engages in strong electronic coupling with U(VI), a typical "hard acid" ion. The simulated results (Figures 3C1–C3) showed that the interaction distance between U=O and S=O in the adsorption configuration decreased to 2.64 Å, with the S-O bond length measured at 1.53 Å, accompanied by a notable redistribution of electron density. These findings indicate that the sulfur site participates in the formation of a stable inner-sphere coordination structure. Energy calculations indicated that the coordination energy reached as high as 19.89 kcal/mol, surpassing that of conventional adsorption sites such as carboxyl or hydroxyl groups. This stable configuration not only contributes to an increased maximum adsorption capacity for U(VI) but also enhances the irreversibility of binding and the material's resistance to interference from competing ions. In addition, sulfur doping may also facilitate electron transfer processes in certain structural systems. In the N, P, and S co-doped carbon material synthesized by Liu et al. (2020), some sulfur sites were present in low-valence states, such as in C-S-C or S^{2-} environments. XPS analysis revealed characteristic peaks of U(IV) after U(VI) adsorption, indicating that partial reduction reactions may have occurred at the material interface. The study further proposed that the local electron density enrichment induced by sulfur doping facilitated the formation of reductive regions on the carbon surface, providing an electron source for the interfacial transformation of U(VI). This suggests that, in specific co-doped systems, electron-rich regions generated by sulfur doping can directly reduce U(VI) to U(IV) during the adsorption process, endowing the material with dual functionalities for simultaneous uranium adsorption and reduction.

4 Enhancing anti-interference capability and selective electrosorption

Uranium-contaminated wastewater typically contains various coexisting metal ions and coordinating anions, making selectivity and anti-interference capability critical factors for the practical application of uranium adsorbents. One effective strategy to improve selectivity is the introduction of functional groups with specific affinity toward uranyl ions on the surface of carbon materials, enabling the selective capture of U(VI) through chemical coordination (Cai et al., 2025; Liu et al., 2024d). These functional groups not only provide additional complexation sites but also modulate the surface charge distribution and wettability of the material, thereby enhancing its compatibility with uranyl ion binding (Yan G. et al., 2025). Studies have shown that U(VI), as a typical Lewis acid, possesses a high charge density and strong hard acid characteristics, making it prone to coordination with electron-donating elements such as oxygen, nitrogen, and phosphorus (Morsy et al., 2019). Common functional groups include amidoxime (Lu et al., 2017), amino (Wang et al., 2020), carboxyl (Jin et al., 2018), and phosphate (Xia et al., 2025), all of which can form stable surface complexes with U(VI) through multidentate coordination. This section focuses on adsorption-oriented strategies and introduces the modification methods and performance of four representative classes of functionalized carbon materials, aiming to elucidate how these groups enhance anti-interference capability and enable selective electrosorption of U(VI).

4.1 Amidoxime functionalization

Among various functional groups, amidoxime has been widely employed for surface modification of carbon-based materials due to its outstanding coordination selectivity and binding stability toward uranyl ions (UO_2^{2+}). This group contains both amino and oxime moieties, which serve as dual coordination sites capable of forming stable bidentate inner-sphere complexes with UO_2^{2+}, thereby significantly enhancing the adsorption capacity and selectivity of carbon-based materials (Wang et al., 2015; Zhang D. et al., 2022). In addition, amidoxime functional groups exhibit strong acid-base tolerance, allowing them to remain stable under neutral to mildly acidic conditions and demonstrating excellent anti-interference performance in complex aqueous systems. From an electronic structure perspective, the nitrogen and oxygen atoms in the amidoxime moiety can donate lone pair electrons, preferentially coordinating with the central uranium atom (U^{6+}) in the uranyl ion to form stable five- or six-membered chelate rings. Moreover, the density and spatial distribution of these functional groups, as well as their interactions with the carbon-based support, significantly influence the recognition and capture efficiency of U(VI). Studies have shown that amidoxime chains aligned within ordered mesoporous carbon frameworks can simultaneously preserve specific surface area and expose coordination sites, thereby enhancing overall adsorption performance (Zhang Z. et al., 2018).

Zhang Z. et al. (2018) used CMK-3 as a hard template and introduced 2-butenenitrile monomers and initiators into the mesoporous channels, where *in situ* polymerization yielded an intermediate with a polyacrylonitrile framework, denoted as xCN-OMC. Subsequent treatment with hydroxylamine hydrochloride solution induced amidoximation, resulting in the formation of the target material AO^{-}OMC (Figure 5A). Structural analysis revealed that the material possessed well-ordered mesoporous channels and a homogeneous distribution of functional groups, with a polymer loading of approximately 16.8%. Adsorption experiments showed that AO-OMC exhibited a maximum U(VI) adsorption capacity of 322.6 mg/g at pH = 5.0, which was significantly higher than that of unmodified CMK-3 (43.4 mg/g). In addition, the material demonstrated strong selectivity for uranium in the presence of competing metal ions (Figure 5B), indicating excellent anti-interference capability and promising application potential. Similarly, Wang et al. (2015) synthesized graphene oxide nanoribbons (GONRs) derived from exfoliated carbon nanotubes and functionalized their edge sites with amidoxime groups to construct the AOGONR material. This material exhibited a maximum U(VI) adsorption capacity of 502.6 mg/g at pH = 4.5. The adsorption process was characterized by rapid kinetics, endothermic behavior, and inner-sphere complexation, highlighting the dominant contribution of the introduced functional sites.

It is worth noting that although amidoxime functional groups exhibit strong complexation capability, their introduction typically involves a relatively complex synthesis process, including cyano group incorporation and subsequent conversion via hydroxylamine treatment, followed by post-processing steps, which can reduce the efficiency of large-scale production. Moreover, due to their exceptionally high affinity for U(VI), amidoxime groups may lead to strong or partially irreversible binding during repeated adsorption-desorption cycles, potentially compromising the reusability of the material. As a result, researchers are actively exploring synergistic modifications combining amidoxime with other functional groups to achieve a balanced enhancement in adsorption capacity, selectivity, and regenerability.

4.2 Amino functionalization

Amino groups ($-NH_2$) are common and highly reactive nitrogen-containing functional groups that can provide effective coordination sites on the surface of carbon-based materials for the capture of U(VI) ions. Studies have shown that amino groups can donate lone pair electrons to the central uranium atom in the uranyl ion (UO_2^{2+}), forming stable N→U coordination bonds, thereby significantly enhancing the material's uranyl-binding affinity and selectivity. In addition, amino groups impart favorable hydrophilicity to the material, which improves surface wettability and the interfacial diffusion environment, thereby indirectly promoting the adsorption process (Wang et al., 2020).

On the one hand, $-NH_2$ groups can remain in a non-protonated state under mildly acidic conditions, ensuring sustained coordination with uranyl ions. On the other hand, their small molecular size and flexible rotational degrees of freedom facilitate efficient spatial positioning around UO_2^{2+} within confined pore environments or surface regions, enabling the formation of stable inner-sphere coordination complexes. These characteristics allow amino groups to perform effectively not only in single-ligand systems but also to exhibit relatively high selectivity in complex systems containing competing ions. Wang et al. (2020) covalently grafted triethylenetetramine (TETA) onto the surface of single-walled carbon nanohorns (SWCNHs) through a two-step reaction. First, carboxyl groups were introduced by nitric acid treatment to obtain SWCNH-COOH, followed by an amide coupling reaction facilitated by EDC/NHS chemistry, enabling the successful anchoring of TETA molecules—rich in amino functionalities—onto the carbon nanohorn surface (Figure 5C). The resulting material (SWCNH-TETA) exhibited significantly enhanced U(VI) adsorption performance in aqueous solution, achieving a maximum adsorption capacity of 333.13 mg/g, which far exceeded that of the carboxylated SWCNH-COOH counterpart (approximately 90.9 mg/g). More importantly, under multi-ion coexistence conditions, SWCNH-TETA maintained outstanding selectivity toward U(VI), with an equilibrium adsorption capacity exceeding 150 mg/g, while exhibiting negligible uptake for interfering ions such as Zn^{2+}, Ni^{2+}, and Mn^{2+} (Figure 5D). These results clearly demonstrate the critical role of nitrogen coordination sites introduced by TETA in enhancing both target-specific binding and selective recognition. In addition, XPS analysis revealed pronounced shifts in the N 1s binding energy after adsorption, further confirming the involvement of amino groups in the formation of stable coordination interactions.

However, the coordination capability of amino groups remains somewhat limited, particularly in systems containing strongly competing ions, where they are susceptible to interference from more potent complexing groups such as carboxylates and phosphates. To address this, some studies have explored further functionalizing amino groups into amide or amidoxime structures

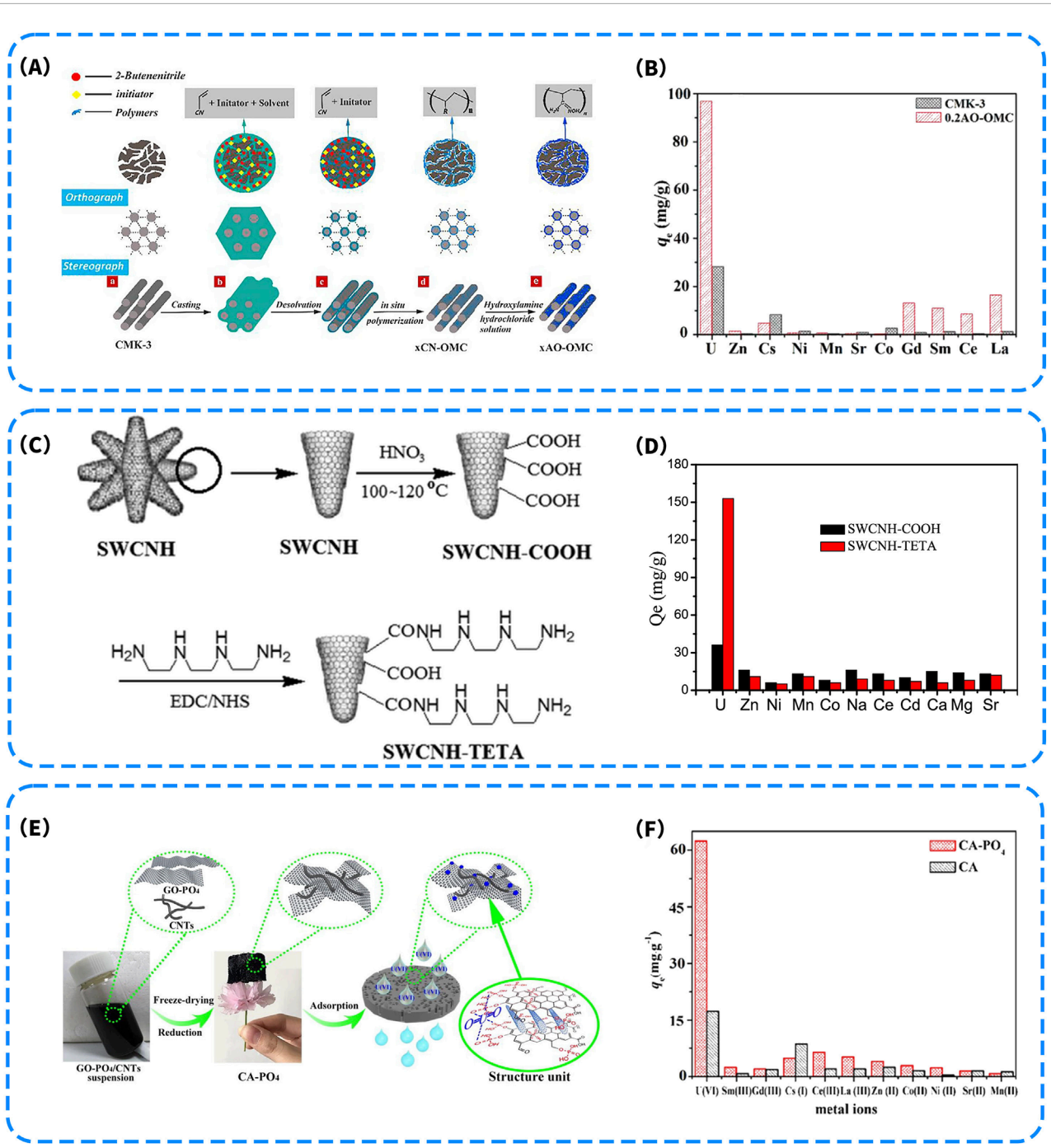

FIGURE 5
(A) Schematic illustration for the synthesis of xAO-OMC; **(B)** Competitive adsorption capacities of coexistent ions on CMK-3 and 0.2AO-OMC (m = 0.010 g, V = 25 mL, C_0 = 0.5 mmol L^{-1}, T = 298.15 K, pH = 5) (Zhang Z. et al., 2018). **(C)** Preparation Process of SWCNH-COOH and SWCNH-TETA; **(D)** Selective adsorption capacity of coexisting ions on two sorbents (C_0 = 60 mg/L, m = 0.01 g, V = 50 mL, T = 303 K, t = 180 min, and pH = 6.0) (Wang et al., 2020). **(E)** Schematic illustration of the preparation process of CA-PO_4 and its coordination adsorption mechanism for U(VI); **(F)** Comparison of sorption capacities of coexisting cations on CA and CA-PO_4 (pH: 5.5, C0: 0.5 mmol L^{-1}, m/V = 0.4 g L^{-1} and T: 298 K) (Zhang et al., 2019).

to enhance binding strength and selectivity. In addition, researchers have also combined amino groups with multidentate ligands such as phosphonates to construct dual-mechanism materials based on "anchoring plus coordination," thereby improving the overall adsorption performance.

4.3 Carboxyl functionalization

Carboxyl groups (-COOH), as common oxygen-containing polar moieties, have been widely employed in the surface functionalization of carbon-based materials to enhance their

affinity toward uranyl ions (UO_2^{2+}). The carbonyl and hydroxyl oxygen atoms within the -COOH group can donate lone pair electrons to form stable inner-sphere complexes with UO_2^{2+}, typically coordinating in a monodentate or bidentate fashion within the uranyl coordination shell. Under mildly acidic to neutral conditions (pH = 4–6), carboxyl groups can deprotonate to $-COO^-$, exhibiting pronounced hard base characteristics that favor the formation of surface complexes with U(VI) possessing high stability constants. This coordination mechanism underlies the selective and often irreversible adsorption behavior of carboxyl groups toward uranium. Supporting spectroscopic evidence has shown that upon U(VI) adsorption, the intensity of C=O and -COOH signals decreases and corresponding binding energies shift, indicating electron density transfer from the carboxyl group to the uranyl center and the formation of stable chemical bonds (Jin et al., 2018; Zhang et al., 2013).

In adsorption environments, the introduction of $-COO^-$ groups significantly shifts the surface potential of the material toward more negative values, thereby enhancing the electrostatic enrichment of UO_2^{2+} and shortening its diffusion path to the active sites. This modulation mechanism markedly promotes the initial adsorption kinetics, particularly under conditions of low uranium concentration or high ionic strength. The study by Jin et al. (2018) demonstrated that nitric acid oxidation significantly increased the surface carboxyl group density of biochar materials, leading to a marked decrease in Zeta potential and a substantial enhancement in the maximum U(VI) adsorption capacity, from 8.9 mg/g to 355.6 mg/g. The introduction of carboxyl groups imparted strong polarity to the material, improving the contact efficiency between hydrated uranyl ions and the porous framework, thereby facilitating the diffusion and interaction of UO_2^{2+} within the pore channels. This improvement in interfacial physicochemical properties further enhanced the adsorption rate and mitigated the diffusion-limited effect on adsorption capacity. The carboxyl-enriched carbon spheres constructed by Zhang et al. (2013), prepared via low-temperature air thermal treatment, exhibited favorable kinetic response and structural stability at pH = 7. The material achieved a maximum U(VI) adsorption capacity of 179.95 mg/g and maintained high selectivity in the presence of various coexisting ions such as Na^+, Ni^{2+}, and Sr^{2+}. The reduction in adsorption capacity was minimal, indicating good selectivity and anti-interference performance.

It is worth noting that carboxyl groups also play a significant role in the synergistic construction of multifunctional coordination interfaces. Nezhad et al. (2021) designed an activated carbon-based adsorbent functionalized with 2-aminobenzoic acid (ABA), denoted as AC-ABA. Carboxyl groups were first introduced via APS oxidation, followed by covalent grafting of ABA through amide bond formation using a DCC coupling agent (Figure 6A), resulting in the co-functionalization of the material surface with both carboxyl and amino coordination groups. This dual-functional architecture not only enhanced the coordination affinity toward U(VI) but also facilitated the modulation of electron density distribution, thereby improving selective recognition and binding strength. In a simulated radioactive wastewater treatment process (Figure 6B), AC-ABA exhibited excellent uranium selectivity and recovery capacity. Uranium could be efficiently desorbed by simple acid washing (pH < 2), allowing the material to be reused, thus demonstrating good sustainability. SEM characterization revealed that the modified material exhibited a more regular pore structure with unobstructed channels (Figures 6C,D), which favored the diffusion of uranyl ions. Further adsorption performance tests showed that AC-ABA achieved a maximum U(VI) adsorption capacity of approximately 197 mg/g under optimal conditions (pH ≈ 5, T = 40 °C), significantly higher than that of unmodified AC (approximately 50 mg/g) (Figures 6E,F). These results clearly highlight the pivotal role of carboxyl groups in the co-construction of multi-site coordination interfaces, particularly when combined with amino functionalities. The enhanced electron-donating ability and complexation stability contributed to the remarkable improvement in selective adsorption performance and application potential. Similarly, Jiao et al. (2023) employed lignin as a carbon precursor and introduced carboxyl and phosphate groups in a synergistic manner following a pre-oxidation treatment to enhance surface reactivity. This process yielded an ordered carbon aerogel with vertically oriented structures, enabling the co-anchoring of multiple functional groups onto the carbon framework. The resulting material exhibited significantly improved polarity and hydrophilicity, which facilitated the formation of tridentate or multidentate coordination complexes. As a result, the material achieved an ultrahigh U(VI) adsorption capacity of 1308.87 mg/g under strong acidic conditions, far surpassing that of single-functionalized systems. Notably, the material also exhibited a photothermal-assisted adsorption effect under UV irradiation, which played a critical role in achieving such exceptional adsorption performance. Therefore, photothermal enhancement offers a novel approach to improve adsorption performance. In addition to the synergistic effect of functional groups, the application of external energy fields such as photothermal stimulation provides a new direction for multi-modal optimization strategies.

4.4 Phosphonate functionalization

Phosphonate groups have emerged as a key direction for the surface functionalization of carbon-based materials in recent years due to their excellent coordination capabilities and high selectivity toward uranyl ions. Phosphorus atoms exhibit a pentavalent state, in which the P=O and P-OH moieties serve as critical reactive sites with strong coordination abilities and favorable charge regulation properties. Under neutral to mildly acidic conditions, these functional groups can form stable inner-sphere complexes with UO_2^{2+} through the lone pair electrons of oxygen atoms, while simultaneously establishing a locally negative electrostatic environment on the material surface. This dual mechanism enhances the electrostatic attraction toward uranyl ions, thereby improving both the selectivity and adsorption capacity of the material (Xia et al., 2025).

Zhang et al. (2019) developed a phosphorylated graphene/carbon nanotube composite aerogel (CA-PO_4) via a one-step freeze-drying and reduction assembly strategy (Figure 5E). The material was fabricated by co-dispersing phosphate-functionalized graphene oxide (GO-PO4) and carbon nanotubes (CNTs) to form a homogeneous precursor solution, which was subsequently freeze-dried and reduced to obtain a three-dimensional porous CA-PO_4 aerogel. The structural units were enriched with abundant PO_4^{2-} coordination groups, which not only enhanced the electronic affinity and interfacial complexation capability toward U(VI) but

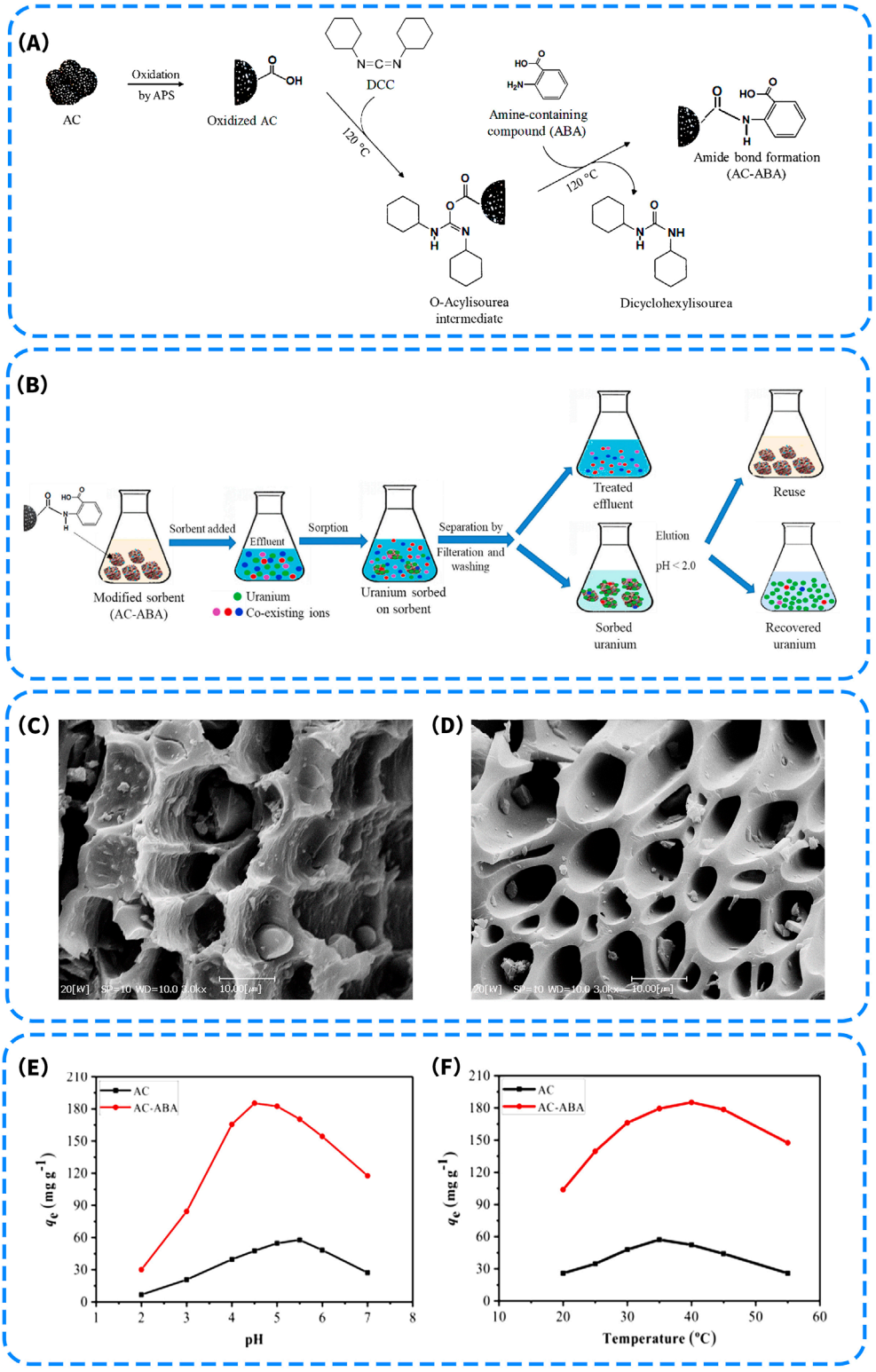

FIGURE 6
(A) Schematic of the surface reactions and synthetic route to AC-ABA; **(B)** The process for uranium removal by the proposed method; Scanning electron micrographs (SEM) of **(C)** AC-ABA and **(D)** AC; The effect of **(E)** pH and **(F)** temperature content on U(VI) uptake by AC and AC-ABA (Nezhad et al., 2021).

also facilitated the directional capture and stable immobilization of UO_2^{2+} through π-π stacking and hydrogen bonding interactions. In adsorption experiments, the material achieved a U(VI) adsorption capacity of 60.6 mg/g, significantly higher than that of the non-phosphorylated control (CA), and exhibited excellent selectivity in the presence of competing rare earth and transition metal ions. Nonspecific adsorption of Sm^{3+}, Gd^{3+}, Cs^+, and Co^{2+} was effectively suppressed (Figure 5F). This study further demonstrates the critical role of phosphate groups in constructing multi-dentate coordination sites and enabling selective recognition of target ions, while also offering a lightweight and efficient approach for uranium removal using carbon-based materials under extreme aqueous conditions.

Compared with conventional carboxyl or amino functionalization, phosphate groups are particularly well-suited for coordinating and immobilizing uranyl ions, which are typical hard acid species. Moreover, phosphate moieties exhibit greater chemical stability than many organic functional groups under acidic conditions, making phosphate modification an important strategy for enhancing the adsorption capacity of carbon-based materials in extreme environments. According to existing literature, the incorporation of phosphate groups not only imparts stronger metal ion coordination ability to carbon-based materials but also enables synergistic improvements in structural stability, adsorption selectivity, and regeneration performance (Husnain et al., 2017).

5 Enhancing the reduction and immobilization efficiency of uranyl ions

For the efficient treatment of uranium-contaminated wastewater, the ideal approach is not only to adsorb and concentrate U(VI) onto the electrode surface, but also to reduce it to lower-valence states and stably immobilize it, thereby minimizing the risk of re-release. Strategies to enhance the reduction and fixation of uranyl ions primarily involve the incorporation of functional metal oxides onto the surface of carbon-based materials, introducing redox-active sites capable of participating in electron transfer reactions. Specifically, metal oxides can form stable inner-sphere complexes with uranyl ions through surface hydroxyl groups, thereby increasing the density of active adsorption sites. Under an applied electric field, they can also facilitate electron donor behavior, promoting the reduction of U(VI) (Figure 7A). In addition, the synergistic interfacial interactions between metal oxides and carbon-based materials contribute to enhanced overall adsorption stability and material recyclability (Yang et al., 2023). Currently, Fe_3O_4 (Zhang J. et al., 2024), MnO_2 (Liao et al., 2019), and TiO_2 (Kou et al., 2025) are the three most widely applied metal oxides for loading onto carbon materials. Their respective mechanisms of action on carbon-based substrates are illustrated in Figures 7B–D. Among them, Fe_3O_4 exhibits excellent performance in electrosorption and magnetic separation due to its relatively good electrical conductivity and magnetic responsiveness. MnO_2, with its multivalent redox capability and high electrochemical activity, can promote electron transfer under an applied electric field, thereby enhancing the synergistic efficiency of U(VI) adsorption and reduction. TiO_2, on the other hand, benefits from its efficient photogenerated electron-hole pair separation and stable semiconductor properties, showing promising potential for the simultaneous removal of uranyl ions and organic contaminants in photoelectrochemical systems. In the following sections, the mechanistic advantages, representative studies, and potential applications of composite systems constructed from these three metal oxides and carbon-based materials for U(VI) adsorption will be discussed in detail.

5.1 Fe_3O_4/carbon composites

Incorporating Fe_3O_4 nanoparticles into carbon-based materials is an effective strategy to enhance their adsorption and removal performance toward U(VI), primarily due to the synergistic effects across interfacial complexation, electrochemical activity, and structural stability. From a surface chemistry perspective, Fe_3O_4 is rich in hydroxyl and Fe-O functional groups, which serve as active sites for forming stable inner-sphere complexes with UO_2^{2+}, thereby improving adsorption strength and selectivity, particularly under neutral to mildly acidic conditions. Moreover, C-O-Fe bridging structures can be formed between Fe_3O_4 and the carbon framework, which not only introduce new electron-donating pathways but also stabilize the dispersion of Fe_3O_4 particles, preventing aggregation and contributing to enhanced material reusability and structural integrity (Chen et al., 2023). Chen et al. (2023) employed a facile "one-can" hydrothermal strategy to *in situ* load Fe_3O_4 nanoparticles onto bamboo-derived biochar, successfully constructing a Fe_3O_4@MBC composite material. SEM images revealed that prior to adsorption, the material surface was uniformly decorated with abundant Fe_3O_4 nanoparticles, forming a rough and porous adsorption interface (Figure 8A). After U(VI) adsorption (Figure 8B), partial aggregation of surface particles and noticeable changes in the pore structure were observed, likely due to the accumulation and complexation deposition of U(VI) on the material surface. The composite exhibited a high BET specific surface area of 129.79 m^2/g and achieved a maximum U(VI) adsorption capacity of 70.45 mg/g at pH = 4.5. XPS analysis showed significant shifts in the binding energies of Fe-O and C=O functional groups before and after adsorption, suggesting their possible involvement in the coordination and adsorption of UO_2^{2+}.

More importantly, the excellent electrical conductivity of Fe_3O_4 enables its outstanding performance in capacitive deionization (CDI) systems by accelerating interfacial electron transfer and facilitating the electrochemical reduction of U(VI) to U(IV). A systematic study by Yang et al. (2023) on Fe_3O_4 @COFs composite electrode materials demonstrated that increasing the Fe_3O_4 loading significantly enhanced both the electrical conductivity and the U(VI) adsorption-reduction capability of the material. XPS survey and high-resolution U 4f spectra (Figures 9A,B) revealed a pronounced increase in U 4f signal intensity after adsorption, with both U(VI) and U(IV) species coexisting, confirming the effective capture and partial reduction of UO_2^{2+} on the material surface. Moreover, changes in the chemical environment of Fe-O and C=N functional groups further indicated their critical roles in coordination complexation and electron transfer processes. Cyclic adsorption-desorption tests showed that the electrode maintained nearly constant adsorption capacity over five cycles (Figure 9C), with U(VI) removal consistently exceeding 70 mg/g.

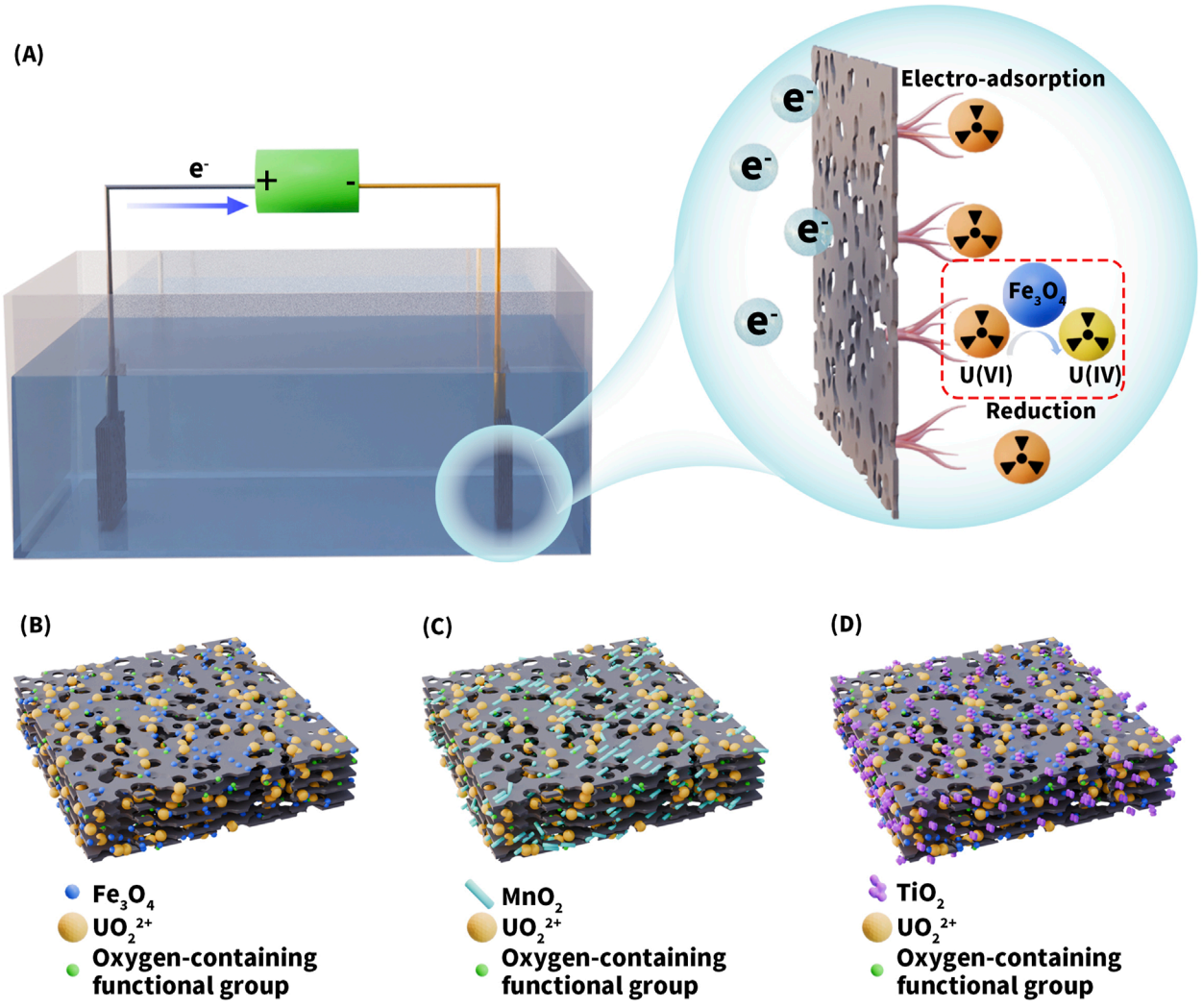

FIGURE 7
(A) Schematic diagram of the CDI uranium removal system and the mechanism of U(VI) capture and reduction by loaded materials. Schematic diagram of the possible loading forms of **(B)** Fe_3O_4, **(C)** MnO_2, and **(D)** TiO_2.

Even after ten consecutive cycles, the adsorption efficiency remained around 85%, demonstrating excellent structural stability and reusability (Figure 9D). Collectively, these results confirm that the incorporation of Fe_3O_4 nanoparticles not only contributes electrons and participates in redox reactions, but also significantly enhances the overall U(VI) removal performance of the CDI system through strong interfacial interactions with the carbon matrix.

5.2 MnO_2/carbon composites

Manganese oxide (MnO_2), owing to the presence of high-valence Mn^{4+} species and its unique crystal structure, exhibits excellent pseudocapacitive behavior and interfacial reactivity in the electrosorptive removal of uranium. On one hand, MnO_2 enables ion storage through the reversible Mn^{4+}/Mn^{3+} redox cycling process. On the other hand, surface Mn-O (H) groups can form inner-sphere complexes with UO_2^{2+}, thereby enhancing adsorption selectivity and stability. Furthermore, the heterointerface structure formed by MnO_2 and carbon-based materials contributes to improved electron transport efficiency, pore structure tunability, and overall material stability (Liu et al., 2024d).

The BC/α-MnO_2-2 composite electrode developed by Liu et al. (2024) exhibited excellent performance in the electrosorption process, achieving a U(VI) loading capacity of 21.35%. SEM images revealed that before adsorption (Figure 8C), the material surface was composed of a three-dimensional cross-linked framework formed by abundant α-MnO_2 nanofibers, creating a uniformly distributed porous structure favorable for ion transport and enhanced specific capacitance. After U(VI) adsorption (Figure 8D), the nanofiber surfaces were extensively covered with uranium deposits, indicating strong capture ability and coordination reactivity. Further electrosorption performance evaluation (Figure 9E) demonstrated that under an applied voltage of 0.9 V, the uranium adsorption capacity of the BC/α-MnO_2-2 composite electrode reached 280.20 mg/g, significantly higher than that of the control without α-MnO_2 loading (75.73 mg/g). This result indicates that the incorporation of α-MnO_2 not only enhanced the pseudocapacitive

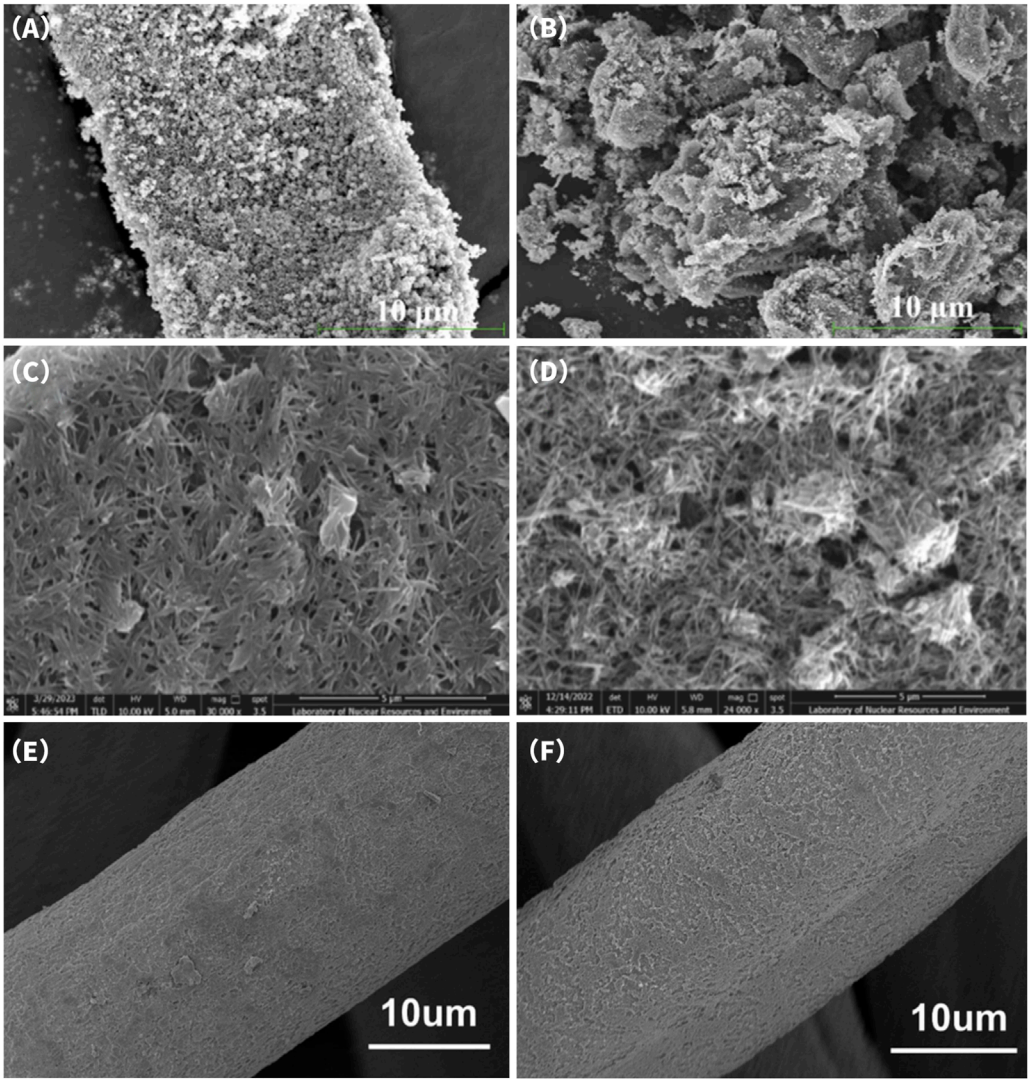

FIGURE 8
SEM images of Fe_3O_4 @MBC-1 **(A)** before U(VI) adsorption; **(B)** after U(VI) adsorption (Chen et al., 2023). SEM images of BC/α-MnO_2-2 **(C)** before U(VI) adsorption; **(D)** after U(VI) adsorption (Liu et al., 2024d). SEM images of CF@TiO_2 **(E)** before U(VI) adsorption; **(F)** after U(VI) adsorption (Cai et al., 2024).

behavior of the material but also introduced additional active sites through Mn^{4+}/Mn^{3+} redox transitions, thereby promoting the effective capture and immobilization of uranyl ions (UO_2^{2+}).

However, when the applied voltage was further increased to 1.2 V (Figure 9F), a slight increase in current was observed, which may be attributed to the enhanced Mn^{4+}/Mn^{3+} redox reactions. At this voltage, the pseudocapacitive response not only effectively promoted the adsorption of uranyl ions but also potentially triggered partial water decomposition, leading to current fluctuations. This observation suggests that although higher voltages can enhance pseudocapacitive activity, they also increase the risk of undesirable side reactions. Therefore, under the optimized condition of 0.9 V, the BC/α-MnO_2-2 composite electrode achieved high uranium adsorption capacity while effectively mitigating side reactions associated with elevated voltages. In contrast to the Mn-N co-doped carbon sphere system, which required 1.8 V to reach saturated adsorption (Jin et al., 2023), the present system exhibited superior U(VI) adsorption performance at just 0.9 V. These findings experimentally validate that loading metal oxides can enhance the pseudocapacitive behavior of electrodes and reduce the energy demand of the electrosorption process.

It is worth emphasizing that the excellent performance of MnO_2 in the electrosorptive removal of uranium arises not only from its intrinsic pseudocapacitive properties but also from its strong interfacial synergy with carbon-based materials. Within the composite structure, MnO_2 can form stable coordination complexes with uranyl ions through surface hydroxyl groups, while simultaneously acting as an electron-active center for the selective reduction of U(VI). Meanwhile, the conductive carbon framework provides pathways for rapid electron transport and charge storage, effectively compensating for the poor conductivity of MnO_2. The three-dimensional conductive network formed through this synergy significantly enhances interfacial reactivity and ion transport efficiency under an applied electric field, thereby improving the overall electrosorption performance and cycling stability of the material (Liao et al., 2019). This strategy

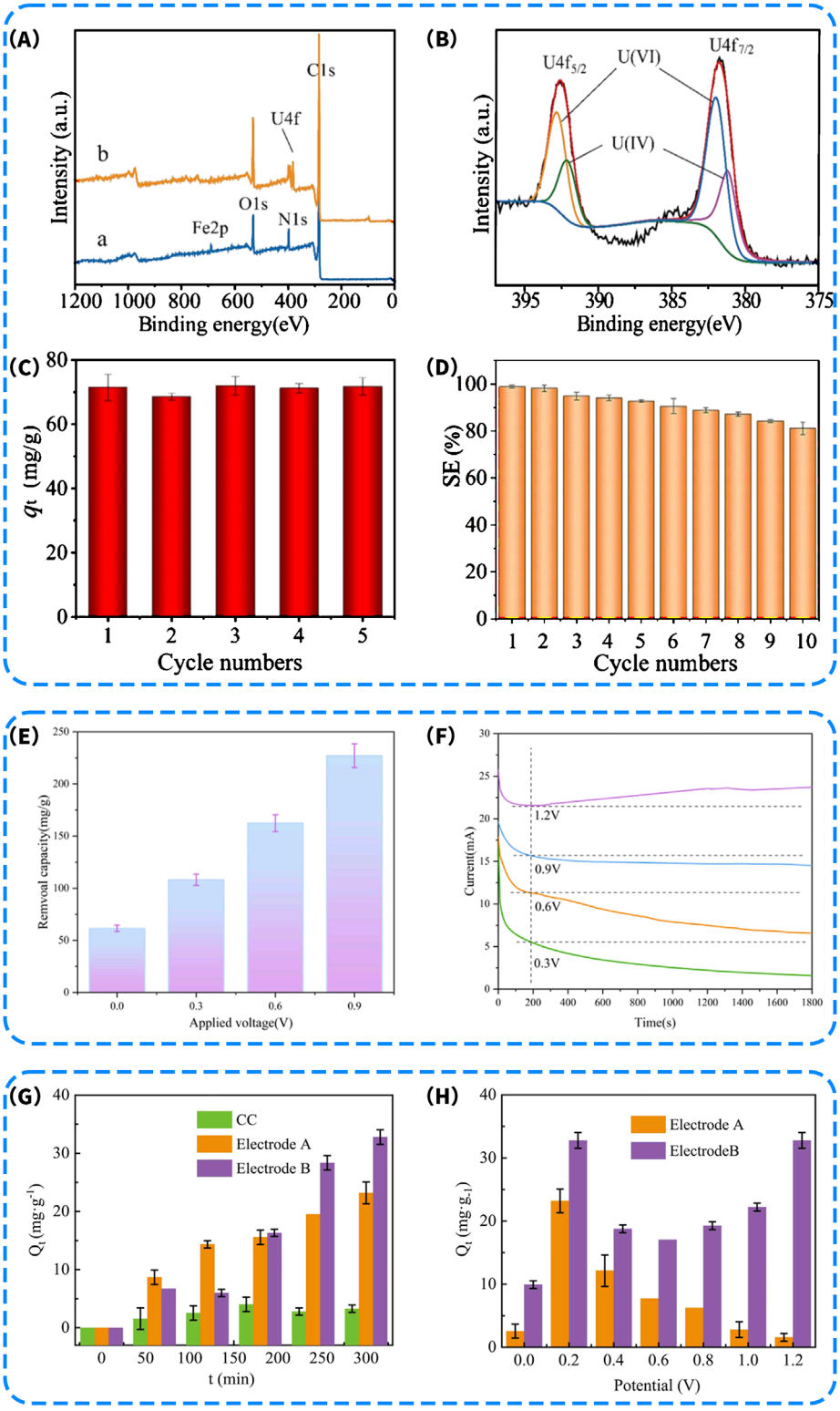

FIGURE 9
(A) XPS survey scan of (a) Fe_3O_4 @COFs and (b) Fe_3O_4 @COFs-U; **(B)** XPS narrow spectra of U 4f after adsorption; **(C)** Recycling performance of Fe_3O_4 @COFs-3 for uranium (VI) sorption after five cycles (Experimental condition: 10.0 mg sorbent, 100 mL solution, 10 mg/L uranium (VI), 1.2 V voltage, pH = 7.0 ± 0.1, 298.15 K); **(D)** Recycling performance of Fe_3O_4 @COFs-3 for uranium (VI) sorption from simulated wastewater containing 1000 ppb of uranium (VI) after five cycles (Experimental condition: 10.0 mg sorbent, 100 mL solution, 1000 ppb of co-existing ions, 1 mol/L NaCl, 1.2 V voltage, pH = 7.0 ± 0.1, 298.15 K) (Yang et al., 2023). **(E)** Impact of applied voltage on U(VI) electrosorption by BC/α-MnO_2-2 at 0.9 V (C_0 = 100 mg/L; pH = 4.0; T = 298 K; t = 2 h); **(F)** Potentiostatic polarization of BC/α-MnO_2-2 (C_0 = 100 mg/L; pH = 4.0) (Liu et al., 2024d). Uranium separation capacity of CDI containing different TiO_2-CC cathodes under different conditions, **(G)** the effect of different cathodes treating 5.0 mg/L uranium solution at 0.20 V, pH = 4.0, t = around 5 h; **(H)** cathodes at different voltages treating 5 mg/L uranium solution at 0.20 V, pH = 4.0, t = around 24 h (Kou et al., 2025).

has been validated in various carbon-based systems, indicating that regulating the interfacial configuration and functional group distribution between metal oxides and carbon frameworks holds great promise for achieving efficient, stable, and regenerable electrosorptive removal of U(VI).

5.3 TiO_2/carbon composites

Loading TiO_2 onto carbon-based materials represents a synergistic enhancement strategy that integrates photochemical, electrochemical, and chemical functionalities, offering significant advantages, particularly in the electrosorption and photocatalytic reduction of uranium. TiO_2 possesses abundant surface hydroxyl groups, which readily participate in inner-sphere complexation with UO_2^{2+} in aqueous environments, thereby enhancing the material's affinity and selectivity toward uranyl ions (Kou et al., 2025). In addition, TiO_2 exhibits strong water adsorption and dissociation capabilities, which facilitate the formation of Ti-OH groups. These groups not only serve as stable coordination sites for uranyl ions, but also promote interfacial charge transfer and electron injection—features that are particularly critical in electrochemical reduction systems (Guo et al., 2024). On the other hand, under light irradiation, TiO_2 can generate electron-hole pairs, where the conduction band electrons possess strong reducing power capable of converting U(VI) into insoluble U(IV), which subsequently deposits on the electrode surface, thereby achieving the separation and enrichment of uranium. Meanwhile, the valence band holes can oxidize organic pollutants, endowing the system with the dual capability of simultaneously removing uranium and organic contaminants (Cai et al., 2024).

However, the inherently poor electrical conductivity of TiO_2 limits its electron transfer efficiency. To overcome this drawback, TiO_2 is often combined with conductive carbon materials to form heterostructures, such as TiO_2 @MXene and TiO_2 @carbon felt, in order to enhance interfacial synergistic effects. Guo et al. (2024) fabricated a TiO2@MXene composite electrode via an *in situ* pyrolysis method and found that the presence of TiO2 significantly promoted the interfacial capture and selective reduction of UO_2^{2+}. The removal efficiency reached 99.7% within 90 min in simulated wastewater and 99.1% within 60 min in simulated seawater, accompanied by the formation of UO_2 and U_3O_8 precipitates. These results confirmed that the formation of Ti-O-U complexes through coordination between Ti-OH groups and UO_2^{2+} was one of the key mechanisms. In another study, Cai et al. (2024) designed a self-powered photoelectrocatalytic (PEC) system based on CF@TiO_2, in which the TiO_2 photoanode harvests solar energy and generates photogenerated electrons that are subsequently transferred along the conductive carbon felt substrate to the cathode surface, where they participate in the electrochemical reduction of uranyl ions (UO_2^{2+}). The system operates efficiently without the need for an external power supply, achieving a reduction of approximately 49.4% of U(VI) to U(IV), thereby confirming the synergistic effect between the surface-active sites of TiO_2 and the photogenerated electrons. SEM images further revealed the microstructural changes of the material during the adsorption process. Prior to adsorption (Figure 8E), the carbon felt surface appeared dense, uniform, and structurally intact, with a stable coating of TiO_2 nanolayers. After adsorption (Figure 8F), particle deposition and slight surface roughening were observed on the fiber surface, indicating the successful capture and partial reduction of U(VI) on the electrode surface. These morphological changes provide visual evidence of the material's outstanding electrocatalytic reduction capability.

In addition to constructing photoelectrocatalytic systems, Kou et al. (2025) synthesized a $Na_2Ti_3O_7/TiO_2$ composite electrode (Electrode B) via a green electrochemical etching method and applied it to an electrosorption system. Experimental results (Figure 9G) showed that under an applied voltage of 0.2 V, Electrode B exhibited a uranium adsorption capacity of 30 mg/g, whereas Electrode A, which lacked $Na_2Ti_3O_7$, only reached 20 mg/g. However, when the voltage was increased to 1.2 V, the adsorption capacity of Electrode A dropped to 15 mg/g, indicating a significant decline. This reduction may be attributed to side reactions such as water splitting at higher voltages, which reduce the number of available active sites. In contrast, Electrode B demonstrated an enhanced capacity of 35 mg/g under 1.2 V (Figure 9H), primarily due to the intercalation/deintercalation channels provided by the layered structure of $Na_2Ti_3O_7$, which effectively sustained pseudocapacitive behavior and offered additional active sites for the capture and immobilization of uranyl ions (UO_2^{2+}). Therefore, by comparing the adsorption capacities of Electrode A and Electrode B under different voltage conditions, it is evident that the incorporation of $Na_2Ti_3O_7$ not only significantly improves electrosorption performance but also effectively mitigates the adverse effects of high-voltage-induced side reactions such as water decomposition. This provides a promising strategy for reducing energy consumption in electrosorption systems.

6 Major challenges and future directions

Significant progress has been made in the application of carbon-based materials for the electrosorptive separation of U(VI) from aqueous solutions. Through structural engineering and functional modification strategies, their adsorption capacity, selectivity, and cycling stability have been continuously improved, demonstrating excellent overall performance. However, most existing studies remain focused on evaluating the effects of individual modification strategies, such as heteroatom doping for electronic structure modulation, surface functionalization for enhancing selective binding, or metal oxide loading for introducing redox activity. A systematic understanding of the synergistic interactions among these strategies is still lacking. This is particularly important given that U(VI) commonly exists in various complex forms in simulated or real wastewater, often coexisting with divalent cations such as calcium and magnesium, or with organic ligands such as humic substances. In such environments, its migration behavior and adsorption mechanisms are influenced by a combination of factors, including electronic distribution, coordination structure, and response to electric fields. As a result, single-pathway strategies are often inadequate, leading to compromised or significantly reduced performance of the materials under complex aqueous conditions.

Emerging research has demonstrated the enhanced efficacy of dual-modification approaches, with preliminary evidence

suggesting even greater performance improvements through ternary synergistic strategies, which consistently exhibit significantly enhanced U(VI) adsorption performance compared to individually modified materials. These findings demonstrate that multifunctional synergistic construction is theoretically feasible and offers substantial performance gains. However, achieving deep integration at the mechanistic level remains challenging. Key issues, such as uniform dopant distribution, enhanced interfacial compatibility, and optimized functional complementarity within the ternary modification system, must be addressed. Future research should therefore focus on developing novel integrated synthesis techniques, such as sol-gel-based co-doping, microwave-assisted multicomponent *in situ* assembly, and layer-by-layer self-assembly, to ensure structural embedding, electronic synergy, and spatial coupling among the three functional elements.

Despite the promising laboratory-scale performance, the large-scale deployment of carbon-based materials for radioactive wastewater treatment faces significant challenges, including cost constraints and long-term stability issues. Most capacitive deionization (CDI) systems have only been evaluated under controlled laboratory conditions using simulated wastewater, with limited validation in complex, real-world radioactive environments (Askari et al., 2024; Song et al., 2023; Wang J. et al., 2025).

A significant limitation lies in synthesizing mesoporous carbon materials, which often rely on hard-template methods involving sacrificial agents (e.g., silica) and hazardous etching processes (e.g., HF or NaOH). These approaches increase fabrication complexity, environmental impact, and safety risks, hindering industrial-scale adoption (Hong et al., 2025; Yan X. et al., 2025). Future research should focus on scalable and environmentally benign synthesis strategies to bridge the gap between lab-scale innovation and practical radioactive wastewater treatment applications.

7 Conclusion

This review comprehensively evaluated the recent progress of carbon-based electrode materials for the electrosorption separation of uranium from aqueous solutions, emphasizing three key modification strategies: heteroatom doping, surface functionalization, and metal oxide loading. These strategies were systematically analyzed regarding their influence on electronic structure, surface chemistry, and uranium-binding mechanisms. A significant finding of this review is that while each modification independently enhances specific aspects of performance-such as conductivity, selectivity, or redox activity, synergistic integration provides significantly greater improvements in adsorption capacity, kinetics, and electrochemical stability than single-modification approaches.

Compared to previous reviews that often treated material optimization strategies in isolation, this work presents a unified framework that links structure-function relationships with practical performance metrics, drawing parallels with advances in energy storage fields such as supercapacitors. This cross-disciplinary perspective underscores the potential of adopting energy material design principles to overcome longstanding challenges in uranium remediation.

Furthermore, the review identifies persistent limitations in current research, such as poor performance in complex water matrices and limited data on long-term electrode stability under realistic operating conditions. Addressing these issues will require future studies integrating scalable synthesis methods, *in situ* characterization, and real-world simulation testing. By emphasizing the need for collaborative innovation across electrochemistry, materials science, and environmental engineering, this work lays a foundation for developing next-generation CDI systems capable of meeting the demands of sustainable radioactive wastewater treatment.

Author contributions

LT: Conceptualization, Writing – review and editing. TW: Conceptualization, Project administration, Writing – original draft. YW: Conceptualization, Funding acquisition, Project administration, Writing – review and editing. YY: Conceptualization, Methodology, Project administration, Writing – review and editing. HZ: Funding acquisition, Writing – review and editing.

Funding

The author(s) declare that financial support was received for the research and/or publication of this article. This work was sponsored by the Research Foundation of China University of Petroleum-Beijing at Karamay (NO. XQZX20230014 and XQZX20250097), Young Science Foundation of Natural Science Foundation of Xinjiang Uygur Autonomous Region (No. 2022D01B146), Science and Technology Plan Project of Xinjiang Uygur Autonomous Region Administration for Market Regulation (No.20241722).

Conflict of interest

The authors declare that the research was conducted in the absence of any commercial or financial relationships that could be construed as a potential conflict of interest.

Generative AI statement

The author(s) declare that no Generative AI was used in the creation of this manuscript.

Publisher's note

References

Ahmad, M., Wu, F., Cui, Y., Zhang, Q., and Zhang, B. (2020). Preparation of novel bifunctional magnetic tubular nanofibers and their application in efficient and irreversible uranium trap from aqueous solution. *ACS Sustain. Chem. Eng.* 8 (21), 7825–7838. doi:10.1021/acssuschemeng.0c00332

Askari, M., Rajabzadeh, S., Tijing, L., and Shon, H. K. (2024). Advances in capacitive deionization (CDI) systems for nutrient recovery from wastewater: paving the path towards a circular economy. *Desalination* 583, 117695. doi:10.1016/j.desal.2024.117695

Bala, R., Karanveer, and Das, D. (2022). Occurrence and behaviour of uranium in the groundwater and potential health risk associated in semi-arid region of Punjab, India. *Groundw. Sustain. Dev.* 17, 100731. doi:10.1016/j.gsd.2022.100731

Cai, S., Wen, Y., Zhang, Q., Zeng, Q., Yang, Q., Gao, B., et al. (2024). Four-in-one multifunctional self-driven photoelectrocatalytic system for water purification: organics degradation, U(VI) reduction, electricity generation and disinfection against bacteria. *Sci. Total Environ.* 928, 172353. doi:10.1016/j.scitotenv.2024.172353

Cai, Y., Li, P., Yuan, Q., Zhao, J., and Tsiakaras, P. (2025). Efficient and selective uranium electrochemical extraction over flexibly engineered bi-functional Polypyrole@MoSe2@MXene. *Chem. Eng. J.* 507, 160496. doi:10.1016/j.cej.2025.160496

Cai, Y., Wu, C., Liu, Z., Zhang, L., Chen, L., Wang, J., et al. (2017). Fabrication of a phosphorylated graphene oxide-chitosan composite for highly effective and selective capture of U(VI). *Environ. Sci. Nano* 4 (9), 1876–1886. doi:10.1039/c7en00412e

Cao, R., Zhang, J., Wang, D., Sun, F., Li, N., and Li, J. (2023). Electrodeposition cobalt sulfide nanosheet on laser-induced graphene as capacitive deionization electrodes for uranium adsorption. *Chem. Eng. J.* 461, 142080. doi:10.1016/j.cej.2023.142080

Chen, D., Zhao, X., Shi, M., Fu, X., Hu, W., Shi, X., et al. (2024). Enhanced and selective uranium extraction onto electrospun nanofibers by regulating the functional groups and photothermal conversion performance. *Chem. Eng. J.* 480, 148108. doi:10.1016/j.cej.2023.148108

Chen, S., Hong, J., Yang, H., and Yang, J. (2013). Adsorption of uranium (VI) from aqueous solution using a novel graphene oxide-activated carbon felt composite. *J. Environ. Radioact.* 126, 253–258. doi:10.1016/j.jenvrad.2013.09.002

Chen, X., Xia, H., Lv, J., Liu, Y., Li, Y., Xu, L., et al. (2023). Magnetic hydrothermal biochar for efficient enrichment of uranium(VI) by embedding Fe3O4 nanoparticles on bamboo materials from "one-can" strategy. *Colloids Surfaces A Physicochem. Eng. Aspects* 658, 130748. doi:10.1016/j.colsurfa.2022.130748

Chen, Y., Hong, Y., Huang, D., Dai, X., Zhang, M., Liu, Y., et al. (2022). Risk assessment management and emergency plan for uranium tailings pond. *J. Radiat. Res. Appl. Sci.* 15 (3), 83–90. doi:10.1016/j.jrras.2022.06.005

Chen, Z., Chen, W., Jia, D., Liu, Y., Zhang, A., Wen, T., et al. (2018). N, P, and S codoped graphene-like carbon nanosheets for ultrafast uranium (VI) capture with high capacity. *Adv. Sci.* 5 (10), 1800235. doi:10.1002/advs.201800235

Cheng, Y., Xu, Y., Mao, H., Zhou, J., Liu, S., Chen, W., et al. (2024). Nitrogen-doped carbon nanotube encapsulated Co9S8 composite cathode for high-selective capacitive extraction of uranium (VI) from radioactive wastewater. *Sep. Purif. Technol.* 342, 127020. doi:10.1016/j.seppur.2024.127020

Dong, W., and Brooks, S. C. (2006). Determination of the formation constants of ternary complexes of uranyl and carbonate with alkaline Earth metals (mg2+, Ca2+, Sr 2+, and Ba2+) using anion exchange method. *Environ. Sci. Technol.* 40 (15), 4689–4695. doi:10.1021/es0606327

Dong, Z., Jiao, X., Baccolo, G., Qin, X., and Yan, Y. (2025). Insight into radionuclide 235U deposition in multiple-environmental media in Muztagh Ata glacier basin of the eastern pamirs. *J. Hazard. Mater.* 486, 137120. doi:10.1016/j.jhazmat.2025.137120

Dubey, S. P., Dwivedi, A. D., Kim, I. C., Sillanpaa, M., Kwon, Y. N., and Lee, C. (2014). Synthesis of graphene-carbon sphere hybrid aerogel with silver nanoparticles and its catalytic and adsorption applications. *Chem. Eng. J.* 244, 160–167. doi:10.1016/j.cej.2014.01.042

Duster, T. A., Szymanowski, J. E. S., and Fein, J. B. (2017). Experimental measurements and surface complexation modeling of U(VI) adsorption onto multilayered graphene oxide: the importance of adsorbate-adsorbent ratios. *Environ. Sci. Technol.* 51 (15), 8510–8518. doi:10.1021/acs.est.6b05776

Elhefnawy, O. A., and Elabd, A. A. (2024). Highly efficient elimination of uranium (VI) and thorium (IV) from aqueous solution using activated carbon immobilized on polystyrene. *Pigment Resin Technol.* 53 (5), 576–586. doi:10.1108/PRT-09-2022-0107

Fan, Y., Yu, J., Chen, J., Zhang, J., Liang, Y., Song, H., et al. (2025). Tuning interlayer spacing and structural disorder in graphene nanosheets *via* organic amine-functionalization to construct hierarchical porous carbons for boosting capacitive deionization. *Desalination* 600, 118469. doi:10.1016/j.desal.2024.118469

Gavrilescu, M., Pavel, L. V., and Cretescu, I. (2009). Characterization and remediation of soils contaminated with uranium. *J. Hazard. Mater.* 163 (2), 475–510. doi:10.1016/j.jhazmat.2008.07.103

Giraldo, L., Serafin, J., Dziejarski, B., and Moreno-Piraján, J. C. (2025). Activated carbon from biomass waste as potential materials for uranium removal. *Chem. Eng. Sci.* 306, 121222. doi:10.1016/j.ces.2025.121222

Gomes, A. F. S., Lopez, D. L., and Ladeira, A. C. Q. (2012). Characterization and assessment of chemical modifications of metal-bearing sludges arising from unsuitable disposal. *J. Hazard. Mater.* 199-200, 418–425. doi:10.1016/j.jhazmat.2011.11.039

Gu, Z. X., Tu, C. N., Wang, Y., Yang, J. J., Liu, N., Liao, J. L., et al. (2015). Preparation of carbon aerogels and adsorption of uranium(VI) from aqueous solution. *Wuli Huaxue Xuebao/Acta Phys. - Chim. Sin.* 31, 95–100. doi:10.3866/PKU.WHXB2014Ac13

Guo, D., Yan, C., Zhu, Y., Huang, B., Qian, Y., and Jin, T. (2025). Phytic acid-induced amorphous and porous transformation of MnO2@GO with enhanced capacitive performance for efficient uranium removal *via* capacitive deionization. *J. Environ. Chem. Eng.* 13 (3), 116672. doi:10.1016/j.jece.2025.116672

Guo, L., Liu, Y. L., Zeng, Q., Zhang, C., Wen, Y., Zhang, Q., et al. (2024). A self-driven solar coupling system with TiO2@MXene cathode for effectively eliminating uranium and organics from complex wastewater accompanying with electricity generation. *J. Hazard. Mater.* 465, 133415. doi:10.1016/j.jhazmat.2023.133415

Hansson, E., Pettersson, H. B. L., Fortin, C., and Eriksson, M. (2017). Uranium aerosols at a nuclear fuel fabrication plant: characterization using scanning electron microscopy and energy dispersive X-ray spectroscopy. *Spectrochim. Acta Part B At. Spectrosc.* 131, 130–137. doi:10.1016/j.sab.2017.03.002

Hilmi, D., Zaim, S., Mortadi, A., Sabir, I., Monkade, M., Nmila, R., et al. (2024). Complex conductivity as a tool to investigate the electrical behavior between graphene oxide and reduced graphene in supercapacitors: correlation between the electrical properties. *Results Eng.* 23, 102673. doi:10.1016/j.rineng.2024.102673

Hong, C., Huang, C., Han, L., Wang, F., Chen, G., Song, Y., et al. (2025). Batch preparation of low-cost photothermal amidoxime-based fabric adsorbent for boosting uranium extraction from seawater. *Sep. Purif. Technol.* 362, 131706. doi:10.1016/j.seppur.2025.131706

Hu, X., Wang, Y., Yang, J. O., Li, Y., Wu, P., Zhang, H., et al. (2020). Synthesis of graphene oxide nanoribbons/chitosan composite membranes for the removal of uranium from aqueous solutions. *Front. Chem. Sci. Eng.* 14 (6), 1029–1038. doi:10.1007/s11705-019-1898-9

Husnain, S. M., Kim, H. J., Um, W., Chang, Y. Y., and Chang, Y. S. (2017). Superparamagnetic adsorbent based on phosphonate grafted mesoporous carbon for uranium removal. *Industrial Eng. Chem. Res.* 56 (35), 9821–9830. doi:10.1021/acs.iecr.7b01737

Ji, D., Liu, Y., Ma, H., Bai, Z., Qiao, Z., Ji, D., et al. (2022). Study on uranium adsorption property of carbon nanotubes prepared by molten salt electrolysis. *ACS Sustain. Chem. Eng.* 10 (36), 11990–11999. doi:10.1021/acssuschemeng.2c03451

Jiao, G. J., Ma, J., Hu, J., Wang, X., and Sun, R. (2023). Hierarchical build-up of vertically oriented lignin-based aerogel for photothermally assisted uranium uptake and recovery from acidic wastewater. *J. Hazard. Mater.* 448, 130988. doi:10.1016/j.jhazmat.2023.130988

Jin, J., Li, S., Peng, X., Liu, W., Zhang, C., Yang, Y., et al. (2018). HNO3 modified biochars for uranium (VI) removal from aqueous solution. *Bioresour. Technol.* 256, 247–253. doi:10.1016/j.biortech.2018.02.022

Jin, M., Huang, X., Wang, Z., Chan, V., Hu, J., Wu, A., et al. (2023). Mn, N co-doped carbon nanospheres for efficient capture of uranium (VI) *via* capacitive deionization. *Chemosphere* 342, 140190. doi:10.1016/j.chemosphere.2023.140190

Jing, L., Lu, Y., Jiang, J., Chen, X., Kam, C. W., Wu, Y., et al. (2024). Constructing a high-performance nitrogen-doped three-dimensional framework graphene material for efficient capacitive deionization. *Desalination* 576, 117382. doi:10.1016/j.desal.2024.117382

Kalfa, A., Penki, T. R., Cohen, I., Shpigel, N., Avraham, E., Aurbach, D., et al. (2020). Thermally reduced graphene oxide as an electrode for CDI processes: a compromise between performance and scalability? *Desalination* 492, 114599. doi:10.1016/j.desal.2020.114599

Kausar, S., Yousaf, M., Mir, S., Awwad, N. S., Alturaifi, H. A., and Riaz, F. (2024). Mesoporous materials: synthesis and electrochemical applications. *Electrochem. Commun.* 169, 107836. doi:10.1016/j.elecom.2024.107836

Ke, P., Wu, T., Liu, Y., Zhao, B., Zhong, T., Sun, Z., et al. (2023). Progress in treatment technology of uranium-containing wastewater. *Ind. Water Treat.* 43 (9), 20–31. doi:10.19965/j.cnki.iwt.2022-0630

Kerisit, S., and Liu, C. (2013). Structure, kinetics, and thermodynamics of the aqueous uranyl(VI) cation. *J. Phys. Chem. A* 117 (30), 6421–6432. doi:10.1021/jp404594p

Kim, J. H., Lee, H. I., Yeon, J. W., Jung, Y., and Kim, J. M. (2010). Removal of uranium(VI) from aqueous solutions by nanoporous carbon and its chelating polymer composite. *J. Radioanalytical Nucl. Chem.* 286 (1), 129–133. doi:10.1007/s10967-010-0624-3

Kohli, D. K., Bhartiya, S., Singh, A., Singh, R., Singh, M. K., and Gupta, P. K. (2016). Capacitive deionization of ground water using carbon aerogel based electrodes. *Desalination Water Treat.* 57 (55), 26871–26879. doi:10.1080/19443994.2016.1186430

Kou, J., Wang, Z., Li, M., Zhang, X., Hua, Y., Fang, Q., et al. (2025). Eco-friendly synthesis of TiO2 nanoparticles for improved uranium adsorption in CDI systems. *J. Environ. Chem. Eng.* 13 (1), 115230. doi:10.1016/j.jece.2024.115230

Li, D., Pang, Y., Meng, N., Zhang, Y., Zhang, Z., Yan, X., et al. (2023). Use of steam to prepare super active carbon with large pore volume for efficient capacitive deionization. *Diam. Relat. Mater.* 139, 110338. doi:10.1016/j.diamond.2023.110338

Li, S., Zhao, L., Wang, S., Li, C., Cai, L., Lv, S., et al. (2024). Covalently anchoring phosphorus nitride imide on carbon nanotubes for efficient electrochemical extraction of uranium. *Chem. Eng. J.* 499, 156076. doi:10.1016/j.cej.2024.156076

Liao, W., Wang, H., Li, F., Zhao, C., Liu, J., Liao, J., et al. (2019). MnO 2 -loaded microorganism-derived carbon for U(VI) adsorption from aqueous solution. *Environ. Sci. Pollut. Res.* 26 (4), 3697–3705. doi:10.1007/s11356-018-3887-9

Liu, D., Zhou, L., Liu, Y., Xia, C., Ouyang, J., and Adesina, A. A. (2024a). Electrodeposition fabrication of graphene oxide/α-MnO2/polyaniline hierarchical porous electrodes with large hybrid specific capacitance for efficient U(VI) electrosorption. *J. Environ. Chem. Eng.* 12 (5), 113450. doi:10.1016/j.jece.2024.113450

Liu, K., Cui, J., Feng, A., Chen, J., Mi, L., Yu, Y., et al. (2025a). Pore optimization engineering for enhancing ion storage and capacitive deionization properties of graphene. *Sep. Purif. Technol.* 362, 131778. doi:10.1016/j.seppur.2025.131778

Liu, Q., Li, W., Zhao, W., Tan, L., Jing, X., Liu, J., et al. (2016). Synthesis of ketoxime-functionalized Fe3O4@C core-shell magnetic microspheres for enhanced uranium(VI) removal. *RSC Adv.* 6 (26), 22179–22186. doi:10.1039/c5ra22758e

Liu, W., Huang, Y., Huang, G., Fan, L., Xie, Y., Zhang, Q., et al. (2023). Convenient sorption of uranium by amidoxime-functionalized mesoporous silica with magnetic core from aqueous solution. *J. Mol. Liq.* 375, 121214. doi:10.1016/j.molliq.2023.121214

Liu, Y., Ouyang, Y., Huang, D., Jiang, C., Liu, X., Wang, Y., et al. (2020). N, P and S co-doped carbon materials derived from polyphosphazene for enhanced selective U(VI) adsorption. *Sci. Total Environ.* 706, 136019. doi:10.1016/j.scitotenv.2019.136019

Liu, Y., Tang, X., Zhou, L., Liu, Z., Ouyang, J., Dai, Y., et al. (2022). Nanofabricated chitosan/graphene oxide electrodes for enhancing electrosorptive removal of U(VI) from aqueous solution. *Sep. Purif. Technol.* 290, 120827. doi:10.1016/j.seppur.2022.120827

Liu, Y., Tian, R., Zhang, S., Bo, T., Wang, Z., Zhao, J., et al. (2024b). Capacitive deionization of uranium mediated by dioxygen functionalities in the C = O = C = O segment of polyacrylic acid-functionalized graphene aerogel. *Chem. Eng. J.* 481, 148388. doi:10.1016/j.cej.2023.148388

Liu, Y., Zhou, L., Ouyang, J., Ao, X., Shuang, M., and Adesina, A. A. (2024c). Electrodeposition nanofabrication of carboxylated carbon nanotubes/α-MnO2 nanorods/polypyrrole composites as high hybrid capacitance electrodes for efficient U(VI) electrosorption. *Sep. Purif. Technol.* 334, 125989. doi:10.1016/j.seppur.2023.125989

Liu, Y., Zhou, L., Xie, Y., Ao, X., Ouyang, J., Liu, Z., et al. (2024d). Enhancing U(VI) removal by using biomass-derived hierarchical porous carbon/α-MnO2 nano fiber composites as high hybrid capacitance electrodes for capacitive deionization. *Process Saf. Environ. Prot.* 182, 948–959. doi:10.1016/j.psep.2023.11.063

Lu, X., Zhang, D., Tesfay Reda, A., Liu, C., Yang, Z., Guo, S., et al. (2017). Synthesis of amidoxime-grafted activated carbon fibers for efficient recovery of Uranium(VI) from aqueous solution. *Industrial Eng. Chem. Res.* 56 (41), 11936–11947. doi:10.1021/acs.iecr.7b02690

Mahmoud, M. E., Tharwat, R. M., Abdelfattah, A. M., and Hassan, S. S. M. (2023). U(VI) capture from water-based systems by decorated nanohybrid of Zn-BTC MOF with GQDs-rGO and alginate hydrogel. *J. Environ. Chem. Eng.* 11 (5), 110497. doi:10.1016/j.jece.2023.110497

Mishra, V., Sureshkumar, M. K., Gupta, N., and Kaushik, C. P. (2017). Study on sorption characteristics of uranium onto biochar derived from eucalyptus wood. *Water, Air, Soil Pollut.* 228 (8), 309. doi:10.1007/s11270-017-3480-8

Misra, S. K., Mahatele, A. K., Tripathi, S. C., and Dakshinamoorthy, A. (2009). Studies on the simultaneous removal of dissolved DBP and TBP as well as uranyl ions from aqueous solutions by using micellar-enhanced ultrafiltration technique. *Hydrometallurgy* 96 (1-2), 47–51. doi:10.1016/j.hydromet.2008.07.013

Mittal, H., Alfantazi, A. M., and Alhassan, S. M. (2024). Recent developments in the adsorption of uranium ions from wastewater/seawater using carbon-based adsorbents. *J. Environ. Chem. Eng.* 12 (1), 111705. doi:10.1016/j.jece.2023.111705

Morshedy, A. S., Taha, M. H., Abd El-Aty, D. M., Bakry, A., and El Naggar, A. M. A. (2021). Solid waste sub-driven acidic mesoporous activated carbon structures for efficient uranium capture through the treatment of industrial phosphoric acid. *Environ. Technol. Innov.* 21. doi:10.1016/j.eti.2021.101363

Morsy, A., Taha, M. H., Saeed, M., Waseem, A., Riaz, M. A., and Elmaadawy, M. M. (2019). Isothermal, kinetic, and thermodynamic studies for solid-phase extraction of uranium (VI) *via* hydrazine-impregnated carbon-based material as efficient adsorbent. *Nucl. Sci. Tech.* 30 (11), 167. doi:10.1007/s41365-019-0686-z

Naz, S., Urooj Wasti, S. A., Ali, F., Afzal, S., Alomayri, T., Duru, M. O., et al. (2025). The role of GO and MXenes in enhancement of electrochemical performance of ZIF 8 for supercapacitor applications. *Chem. Inorg. Mater.* 5, 100094. doi:10.1016/j.cinorg.2025.100094

Nezhad, M. M., Semnani, A., Tavakkoli, N., and Shirani, M. (2021). Selective and highly efficient removal of uranium from radioactive effluents by activated carbon functionalized with 2-aminobenzoic acid as a new sorbent. *J. Environ. Manag.* 299, 113587. doi:10.1016/j.jenvman.2021.113587

Ning, Y., Luo, Z., Li, Y., Yang, Z., Liu, D., and Zhang, Y. (2021). Alkaline leaching characteristics of uranium from lincang coal: correlation with the dissolution of coal humic substances. *Fuel* 305, 121507. doi:10.1016/j.fuel.2021.121507

Obodo, R. M., Afzal, S., Sarwar, S. G., Nsude, H. E., Usman, M., Ahmad, I., et al. (2024a). The role of ion beam in modification of CuO@NiO@ZnO/GO electrode for supercapacitor application. *J. Energy Storage* 104, 114471. doi:10.1016/j.est.2024.114471

Obodo, R. M., Mbam, S. M., Iwueke, D. C., Ramzan, M., Ijeh, R., Ahmad, I., et al. (2022a). Annealing optimization of graphitized $_{Co3O4}$@CuO@NiO composite electrodes for supercapacitor applications. *Energy Storage* 4 (5), e347. doi:10.1002/est2.347

Obodo, R. M., Nsude, H. E., Eze, C. U., Okereke, B. O., Ezugwu, S. C., Ahmad, I., et al. (2022b). Optimization of MnO2, NiO and MnO2@NiO electrodes using graphene oxide for supercapacitor applications. *Curr. Res. Green Sustain. Chem.* 5, 100345. doi:10.1016/j.crgsc.2022.100345

Olchowski, R., Podkościelna, B., Zawisza, B., Morlo, K., and Dobrowolski, R. (2023). U(VI) removal from water by novel P-modified activated carbon derived from polymeric microspheres. *Environ. Nanotechnol. Monit. Manag.* 20, 100788. doi:10.1016/j.enmm.2023.100788

Othman, H. Q., and Hussein, Z. A. (2025). Assessment of radionuclide (Radon, radium, and uranium) concentrations and heavy metal levels in blood samples from workers in concrete block factories. *J. Radiat. Res. Appl. Sci.* 18 (1), 101306. doi:10.1016/j.jrras.2025.101306

Ren, Q., Wang, Y., Wang, Y., Feng, Z., Du, Y., Wang, C., et al. (2025a). Inspiring the potential of graphene oxide aerogel for uranium(VI) electrosorption: a precursor reconfiguration strategy and synergistic integration with polyethyleneimine. *Desalination* 609, 118883. doi:10.1016/j.desal.2025.118883

Ren, Q., Wang, Y., Wang, Y., Feng, Z., Jiang, H., Liu, Y., et al. (2025b). Construction of three-dimensional polyethyleneimine incorporated graphene oxide aerogels as high-capacity electrode for enhanced uranium(VI) electrosorption performance. *Sep. Purif. Technol.* 352, 128191. doi:10.1016/j.seppur.2024.128191

Ren, Q., Xia, H., Wang, Y., Lv, J., Yuan, D., Liu, Y., et al. (2024). Novel malonamide-amidoxime bifunctional polymers decorated graphene oxide/chitosan electrode for enhancing electrosorptive removal of uranium(VI). *Sep. Purif. Technol.* 330, 125292. doi:10.1016/j.seppur.2023.125292

Schneider, E., Carlsen, B., Tavrides, E., van der Hoeven, C., and Phathanapirom, U. (2013). A top-down assessment of energy, water and land use in uranium mining, milling, and refining. *Energy Econ.* 40, 911–926. doi:10.1016/j.eneco.2013.08.006

Shehzad, H., Chen, J., Shuang, M. T., Liu, Z., Farooqi, Z. H., Sharif, A., et al. (2024). Insights into electro-assisted and selective adsorption of U(VI) using hierarchical porous and activated biocarbon from lotus pods/2D-MoS2/polypyrrole composites through capacitive deionization. *Process Saf. Environ. Prot.* 181, 354–366. doi:10.1016/j.psep.2023.11.032

Shuang, M., Shehzad, H., Zhou, L., Liu, Z., Ouyang, J., Sharif, A., et al. (2024). Surface-active and templated biocarbon derived from pluronic F-127 and heteroatom-doped sucrose and its WO3 composites with enhanced pseudocapacitance for uranium electrosorption. *J. Environ. Chem. Eng.* 12 (3), 112631. doi:10.1016/j.jece.2024.112631

Song, W., Diaz, F., Yasinskiy, A., Kleinert, T., and Friedrich, B. (2024). Enabling data-driven process dynamic modeling for extractive leaching and chemical precipitation. *Chem. Eng. Res. Des.* 211, 179–183. doi:10.1016/j.cherd.2024.10.004

Song, Y., Wei, G., Kopeć, M., Rao, L., Zhang, Z., Gottlieb, E., et al. (2018). Copolymer-templated synthesis of nitrogen-doped mesoporous carbons for enhanced adsorption of hexavalent chromium and uranium. *ACS Appl. Nano Mater.* 1 (6), 2536–2543. doi:10.1021/acsanm.8b00103

Song, Y., Ye, G., Lu, Y., Chen, J., Wang, J., and Matyjaszewski, K. (2016). Surface-initiated ARGET ATRP of Poly(Glycidyl methacrylate) from carbon nanotubes *via* bioinspired catechol chemistry for efficient adsorption of uranium ions. *ACS Macro Lett.* 5 (3), 382–386. doi:10.1021/acsmacrolett.6b00099

Song, Z., Chen, Y., Ren, N., and Duan, X. (2023). Recent advances in the fixed-electrode capacitive deionization (CDI): innovations in electrode materials and applications. *Environ. Funct. Mater.* 2 (3), 290–303. doi:10.1016/j.efmat.2023.11.001

Suranshe, S. S., and Patil, A. (2023). Strategically improving electrical conductivity of reduced graphene oxide through a series of reduction processes. *Mater. Lett.* 333, 133648. doi:10.1016/j.matlet.2022.133648

Tang, Z., Li, Y., Tan, K., Wang, G., Li, C., Liu, L., et al. (2025). Efficient removal of uranium and sulfate in acid contaminated groundwater by flow electrode capacitive deionization. *Desalination* 594, 118304. doi:10.1016/j.desal.2024.118304

Tauk, M., Bechelany, M., Sistat, P., Habchi, R., Cretin, M., and Zaviska, F. (2024). Ion-selectivity advancements in capacitive deionization: a comprehensive review. *Desalination* 572, 117146. doi:10.1016/j.desal.2023.117146

Van Zile, M., Herminghuysen, K., Kauffman, A., White, S., Kandlakunta, P., Li, S., et al. (2024). Gamma-ray spectra of post-irradiated uranium salt for total mass accounting with sodium-22 tracer. *Prog. Nucl. Energy* 168, 104992. doi:10.1016/j.pnucene.2023.104992

Wang, C., Du, X., Gao, F., Hao, X., and Guan, G. (2024a). Electrochemically switched ion separation technologies: a review on electroactive ion exchange materials and system architectures. *Chem. Eng. J.* 490, 151708. doi:10.1016/j.cej.2024.151708

Wang, C., Huang, D., He, F., Jin, T., Huang, B., Xu, J., et al. (2020). Efficient removal of uranium(VI) from aqueous solutions by triethylenetetramine-functionalized single-walled carbon nanohorns. *ACS Omega* 5 (43), 27789–27799. doi:10.1021/acsomega.0c02715

Wang, R., Li, M., Liu, T., Li, X., Zhou, L., Tang, L., et al. (2022). Encapsulating carbon-coated nano zero-valent iron particles with biomass-derived carbon aerogel for efficient uranium extraction from uranium-containing wastewater. *International Journal of Biological Macromolecules* 364. doi:10.1016/j.jclepro.2022.132654

Wang, C., Yu, G., and Wang, J. (2024b). Treatment of spent radioactive organic solvents from nuclear fuel reprocessing plant: advances and perspectives. *Nucl. Eng. Des.* 422, 113138. doi:10.1016/j.nucengdes.2024.113138

Wang, D., Wang, J., Zhang, D., and Li, J. (2025a). Efficient remediation and synchronous recovery of uranium by phosphate-functionalized magnetic carbon-based flow electrode capacitive deionization. *Water Res.* 281, 123707. doi:10.1016/j.watres.2025.123707

Wang, J., Liu, C., Ding, S., and Yang, Y. (2025b). Capacitive deionization in water treatment: a review of reactor dynamics, electrode materials, functional membranes, and modeling techniques. *Desalination* 600, 118459. doi:10.1016/j.desal.2024.118459

Wang, N., Ding, D., Liu, J., and Zhang, H. (2024c). Characterization of groundwater and cores in the decommissioned acid *in-situ* leach uranium mining area: enlightenment for uranium contaminated groundwater remediation. *J. Environ. Chem. Eng.* 12 (6), 114315. doi:10.1016/j.jece.2024.114315

Wang, S., Wang, H., Huang, X., Wu, Z., Xue, H., and Zhao, C. (2025c). A novel magnetic adsorption and capacitive deionization coupled technology for industrial saline wastewater recycling. *Water Res.* 281, 123559. doi:10.1016/j.watres.2025.123559

Wang, Y., Liu, Y., Hu, X., Li, Y., Tu, H., Wang, C., et al. (2021). Rational structure design for enhanced uranium(VI) capture and beyond: From carbon nanotubes to graphene oxide nanoribbons. *J. Mol. Liq.* 323, 114639. doi:10.1016/j.molliq.2020.114639

Wang, Y., Wang, Z., Ang, R., Yang, J., Liu, N., Liao, J., et al. (2015). Synthesis of amidoximated graphene oxide nanoribbons from unzipping of multiwalled carbon nanotubes for selective separation of uranium(VI). *RSC Adv.* 5 (108), 89309–89318. doi:10.1039/c5ra15977f

Wang, Z., Kou, J., Li, M., Zhang, X., Hua, Y., Fang, Q., et al. (2025d). Enhancement and sustained uranium removal of 2D transition metal sulfide-graphene oxide composite/carbon cloth cathodes in capacitive deionization system. *Desalination* 605, 118745. doi:10.1016/j.desal.2025.118745

Wu, H., Zhang, C., Qiu, Y., and Sun, X.-F. (2024). Synergistic enhancement of electric double layers and faradaic reactions in capacitive deionization: the role of NTP@C composite. *Chem. Eng. J.* 496, 153491. doi:10.1016/j.cej.2024.153491

Wu, L. L., Cao, Y. S., Li, Z. P., Hu, L., Zhang, Z. J., Yu, Q., et al. (2020). Preparation of areca residue activated carbon composite and its adsorption performance for uranium (VI) in wastewater. *Desal. Water Treat.* 182 (4, 144–154). doi:10.5004/dwt.2020.25136

Xia, Z., Zhang, C. R., Chen, X. J., Cai, Y. J., Yi, S. M., Liang, R. P., et al. (2025). Phosphorylated litchi shell-derived biochar for removal U(VI) from mining wastewater. *Chem. Eng. Sci.* 301, 120708. doi:10.1016/j.ces.2024.120708

Xie, T., Zhu, J., Liu, X., Hao, Y., Wang, R., Liang, P., et al. (2025). Fissure channeling caused anomalous uranium concentration in groundwater downstream of a uranium mine tailings impoundment site. *J. Hazard. Mater.* 488, 137492. doi:10.1016/j.jhazmat.2025.137492

Xue, Y., Cao, M., Gao, J., Gui, Y., Chen, J., Liu, P., et al. (2021). Electroadsorption of uranium on amidoxime modified graphite felt. *Sep. Purif. Technol.* 255. doi:10.1016/j.seppur.2020.117753

Yan, G., Zuo, B., Liu, S., Wang, T., Wang, R., Bao, J., et al. (2025a). Opportunities and challenges of capacitive deionization for uranium extraction from seawater. *Acta Physico-Chimica Sin.* 41 (4), 100032. doi:10.3866/PKU.WHXB202404006

Yan, X., Yang, J., Huang, C., Yu, Z., Zhang, H.-X., Fang, L., et al. (2025b). Ultra-fast, cost-effective and scale-up preparation of lightweight electromagnetic interference shielding graphite worm-based aerogel. *Chem. Eng. J.* 504, 158793. doi:10.1016/j.cej.2024.158793

Yang, S., Ye, Z., Cheng, X., Wang, Y., Luan, Z., Li, W., et al. (2023). Electro-adsorption and reduction of Uranium(VI) by Fe3O4@COFs electrode with enhanced removal performance. *Chem. Eng. J.* 474, 145598. doi:10.1016/j.cej.2023.145598

Yousef, A., Hameed, R. M. A., Maafa, I. M., Abutaleb, A., and El-Halwany, M. M. (2025). Silicon carbide-graphene nanocomposite electrodes for enhanced desalination *via* capacitive deionization. *Ceram. Int.* 51, 29633–29644. doi:10.1016/j.ceramint.2025.04.166

Youssef, W. M., El-Maadawy, M. M., Masoud, A. M., Alhindawy, I. G., and Hussein, A. E. M. (2024). Uranium capture from aqueous solution using palm-waste based activated carbon: sorption kinetics and equilibrium. *Environ. Monit. Assess.* 196 (5), 428. doi:10.1007/s10661-024-12560-y

Zhang, C., Li, X., Chen, Z., Wen, T., Huang, S., Hayat, T., et al. (2018a). Synthesis of ordered mesoporous carbonaceous materials and their highly efficient capture of uranium from solutions. *Sci. China Chem.* 61 (3), 281–293. doi:10.1007/s11426-017-9132-7

Zhang, D., Zhao, B., Liu, L., Tang, H., Wang, X., and Yu, S. (2022a). Insights into enhanced elimination of U(VI) and Eu(III) by amidoxime-functionalized Ti3C2T MXenes. *Sep. Purif. Technol.* 294, 121179. doi:10.1016/j.seppur.2022.121179

Zhang, J., Wang, Y., Wei, Y., Xu, M., Hu, Y., and Li, J. (2024). Magnetic CNT-Based electrode for efficient electro-adsorption of uranium. *J. Environ. Chem. Eng.* 12 (2). doi:10.1016/j.jece.2024.112160

Zhang, J., Zhang, N., Tack, F. M. G., Sato, S., Alessi, D. S., Oleszczuk, P., et al. (2021). Modification of ordered mesoporous carbon for removal of environmental contaminants from aqueous phase: a review. *J. Hazard. Mater.* 418, 126266. doi:10.1016/j.jhazmat.2021.126266

Zhang, Q., Wang, Y., Wen, Y., Wang, R., Zhang, Y., and Zeng, Q. (2024). Co/N-codoped carbon nanoplate array coated carbon fiber cathode for solar driven uranium extraction from complex radioactive wastewater. *Desalination* 591. doi:10.1016/j.desal.2024.118014

Zhang, R., Xu, L., Yu, F., Xiao, S., Wang, C., Yuan, D., et al. (2023a). Sulfonated heteroatom co-doped carbon materials with a porous structure boosting electrosorption capacity for uranium (VI) removal. *J. Solid State Chem.* 327, 124262. doi:10.1016/j.jssc.2023.124262

Zhang, X., Liu, R., Wang, H., Liu, L., and Yue, C. (2023b). Fabrication of phosphate-containing mesoporous carbon for fast and efficient uranium (VI) extraction. *Colloids Surfaces A Physicochem. Eng. Aspects* 662, 130994. doi:10.1016/j.colsurfa.2023.130994

Zhang, X., Ni, B., Li, X., Guan, X., Xia, W., Hao, J., et al. (2022b). Synthesis of nickel cobaltite/multiwalled carbon nanotubes composites and their application for removing uranium (VI). *Crystals* 12 (12), 1712. doi:10.3390/cryst12121712

Zhang, Z., Dong, Z., Wang, X., Dai, Y., Cao, X., Wang, Y., et al. (2019). Synthesis of ultralight phosphorylated carbon aerogel for efficient removal of U(VI): Batch and fixed-bed column studies. *Chem. Eng. J.* 370, 1376–1387. doi:10.1016/j.cej.2019.04.012

Zhang, Z., Dong, Z., Wang, X., Ying, D., Niu, F., Cao, X., et al. (2018b). Ordered mesoporous polymer–carbon composites containing amidoxime groups for uranium removal from aqueous solutions. *Chem. Eng. J.* 341, 208–217. doi:10.1016/j.cej.2018.02.044

Zhang, Z. B., Nie, W. B., Li, Q., Xiong, G. X., Cao, X. H., and Liu, Y. H. (2013). Removal of uranium(VI) from aqueous solutions by carboxyl-rich hydrothermal carbon spheres through low-temperature heat treatment in air. *J. Radioanalytical Nucl. Chem.* 298 (1), 361–368. doi:10.1007/s10967-013-2441-y

Zhao, Y., Che, G., Li, X., Lei, T., Pan, Q., Su, Z., et al. (2025). Uranyl-organic framework incorporating Ru(bpy)32+ for improved photoelectrocatalytic U(VI) reduction. *Sep. Purif. Technol.* 356, 130004. doi:10.1016/j.seppur.2024.130004

Zhou, J., Zhang, X., Zhang, Y., Wang, D., Zhou, H., and Li, J. (2022). Effective inspissation of uranium(VI) from radioactive wastewater using flow electrode capacitive deionization. *Sep. Purif. Technol.* 283, 120172. doi:10.1016/j.seppur.2021.120172

Zhu, K., Chen, C., Xu, M., Chen, K., Tan, X., Wakeel, M., et al. (2018a). *In situ* carbothermal reduction synthesis of Fe nanocrystals embedded into N-doped carbon nanospheres for highly efficient U(VI) adsorption and reduction. *Chem. Eng. J.* 331, 395–405. doi:10.1016/j.cej.2017.08.126

Zhu, M., Li, F., Chen, W., Yin, X., Yi, Z., and Zhang, S. (2021). Adsorption of U(VI) from aqueous solution by using KMnO4-modified hazelnut shell activated carbon: characterisation and artificial neural network modelling. *Environ. Sci. Pollut. Res.* 28 (34), 47354–47366. doi:10.1007/s11356-021-14034-x

Zhu, R., Zhang, C., Zhu, L., Liu, L., Bai, J., Wang, Y., et al. (2024). Bis-substituted amino acid functionalized chitosan aerogels: High uranium adsorption capacity and antibacterial properties. *Int. J. Biol. Macromol.* 276. doi:10.1016/j.ijbiomac.2024.133890

Zhu, R., Zhang, C., Zhu, L., Zhang, J., Liu, L., Bai, J., et al. (2025). Porous hierarchical mxene/Chitosan cryogel with synergistic phosphate/amidoxime groups for ultra-efficient uranium adsorption under pH-response behavior. *Chem. Eng. J.* 504, 158181. doi:10.1016/j.cej.2024.158181

Zhu, S., Leng, Y., Yan, M., Tuo, X., Yang, J., Almásy, L., et al. (2018b). Bare and polymer coated iron oxide superparamagnetic nanoparticles for effective removal of U (VI) from acidic and neutral aqueous medium. *Appl. Surf. Sci.* 447, 381–387. doi:10.1016/j.apsusc.2018.04.016